Project N. 037110

NEAREST

Integrated observations from NEAR shore sources of Tsunamis: Towards an early warning system

Instrument: STREP

Thematic priority: 1.1.6.3 GOCE (Global Change and Ecosystems)

D22a: report on the lithology, geochemistry, physical properties and age of offshore seismic deposits

Due date of deliverable: September 2009
Actual submission date: March 2010

Start date of the project: 01/10/2006 Duration: 36 + 6 months

Organisation name of the lead contractor for this deliverable: CSIC

Revision: Final

Project Co founded By the European Commission within the Sixth Framework Programme (2002-2006)		
Dissemination Level		
PU	Public	
PP	Restricted to other programme participants (Including Commission Services)	
RE	Restricted to a group specified by the Consortium (Including Commission Services)	**RE**
CO	Confidential, only for members of the Consortium (Including Commission Services)	

WP6 - Paleotsunami and Paleoseismic records

D22: Report on the lithology, geochemistry, physical properties and age of offshore seismic deposits

Leader Task 6.2: CSIC

Task 6.2 responsible: Dr. Eulàlia Gràcia i Mont

Unitat de Tecnologia Marina - CSIC
Centre Mediterrani d'Investigacions Marines i Ambientals (CMIMA)
Barcelona (Spain)
egracia@cmima.csic.es

Abstract

The SW margin of the Iberian Peninsula hosts the present-day boundary between the Eurasian and African Plates. Convergence (4-5 mm/yr) is accommodated through a wide deformation zone characterized by moderate magnitude seismic activity. This zone has also been the source of the most important seismic events in Western Europe, such as the 1755 Lisbon Earthquake and Tsunami and 1969 Horseshoe Earthquake. Despite efforts to identify active seismogenic structures in the Gulf of Cadiz in the last ten years, little is known about its paleoseismic history. The turbidite paleoseismology approach was applied for the first time in a low-rate convergent margin to determine the recurrence interval of large earthquake events occurred in SW Iberia during the Holocene. A total of 21 sediment cores collected at strategically located basins (i.e. Tagus Abyssal Plain, Infante Don Henrique Basin, Horseshoe and Seine Abyssal Plains) and sediment pathways of the Gulf of Cadiz reveal that these deep-sea basins preserve a record of episodic deposition of turbidites. In the SW Iberian Margin excluding special climatic events, earthquakes are the most likely triggering mechanism for synchronous, widely-spaced distributed turbidites during the Holocene, when sea level was relatively stable. Textural, mineralogical, physical properties and geochemical signatures of turbidite deposits together with its chronology are presented in this report.

1. Introduction

Crustal deformation in the SW margin of the Iberian Peninsula is controlled by the NW-SE convergence of the African and Eurasian Plates (4.5-5.6 mm/yr) at the eastern end of the Azores-Gibraltar zone (e.g. Argus et al., 1989; McClusky et al., 2003). This convergence is accommodated through a wide active deformation zone (e.g. Sartori et al., 1994; Hayward et al., 1999) characterized by low to moderate magnitude seismicity (Udías et al., 1976; Grimison and Chen, 1986; Buforn et al., 1995, 2004; Stich et al., 2005a,b) (Fig. 1). However, great earthquakes (Mw ≥ 8.0) such as the 1755 Lisbon Earthquake and Tsunami and the 1969 Horseshoe Earthquake have also occurred in this region (Fukao, 1973; Buforn et al., 1995, 2004; Baptista et al., 1998; Martínez Solares and López Arroyo, 2004) (Fig. 1). A multidisciplinary marine geological and geophysical dataset acquired during the last ten years offshore southern Portugal revealed a number of active NE-SW trending west-verging folds and thrusts (Zitellini et al., 2001, 2004; Gràcia et al., 2003a; Terrinha et al., 2003) and WNW-ESE strike-slip faults (Rosas et al., 2009; Zitellini et al., 2009; Terrinha et al., 2009) (Fig. 1). Deformed Quaternary units together with swarms of earthquakes associated with seafloor surface ruptures suggest that these faults are active and that they may represent an earthquake and tsunami hazard to the coasts of Portugal, Spain and North Africa (Gràcia et al., 2003a,b; Terrinha et al., 2003, 2009; Zitellini et al., 2004).

Assessment of seismic hazard in SW Iberia is largely based on the relatively short period of instrumental (< 50 years) and historical (< 2000 years) earthquake catalogues (e.g. Peláez and López Casado, 2002). This may not be sufficient to assess seismic hazard models in the Iberian Peninsula, especially when considering high magnitude earthquakes and long recurrence intervals (> 10^3 years) (e.g. Masana et al., 2004; Gràcia et al., 2006; Vizcaino et al., 2006). A submarine paleoseismic approach may allow us to determine past seismic activity and to obtain a recurrence rate for great magnitude earthquakes (Mw ≥ 8.0). In order to investigate the recurrence rate of large Holocene events, such as the Lisbon Earthquake, we tested for the first time the "turbidite paleoseismology" concept (Adams, 1990; Nelson et al., 1996; Goldfinger et al., 2003, 2007) in a low convergence margin.

In this report, we present data from marine sediment cores collected in slope basins and abyssal plains off SW Iberia (Fig. 2). The main objectives are:

1) To recognize submarine channels and depositional basins form the Gulf of Cadiz in order to select sampling sites with high potential of preservation of turbidite deposits;

2) To characterize turbidite deposits on the basis of sedimentary facies, texture, physical properties (magnetic susceptibility, P-wave velocities, density) and geochemical composition;

3) To constrain the age of the turbidites recorded on sedimentary record using radiometric (^{14}C) dating.

Regional correlation of widespread turbidite events with instrumental and historical earthquakes and tsunamis from the Gulf of Cadiz; and determination of recurrence interval of large earthquakes occurred during the Holocene will be presented in report D23.

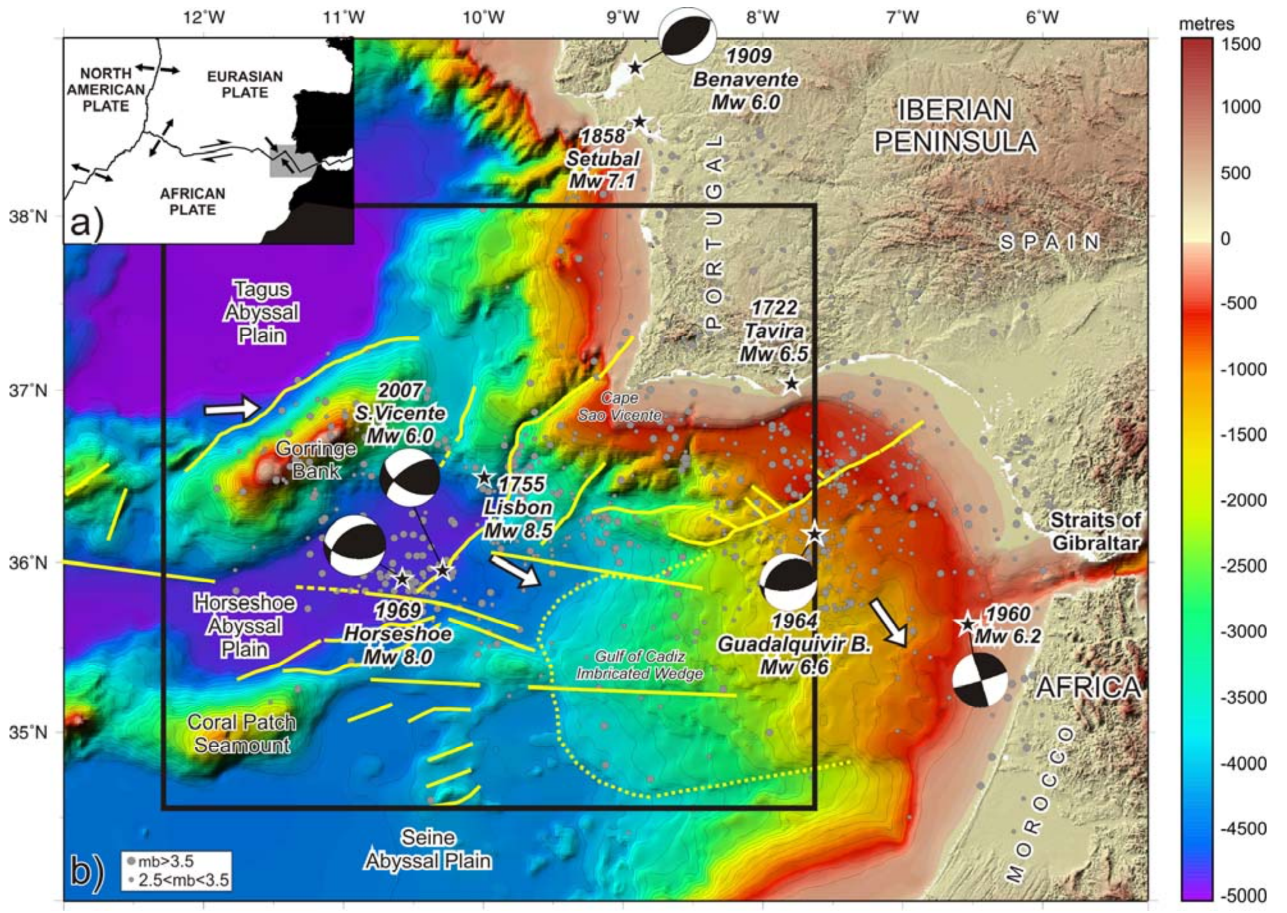

Fig. 1. *Colour shaded relief map of the SW Iberian Margin (contour interval: 200 m). Plate convergence is depicted by the white arrows. Earthquake epicentres are represented by grey dots. Black stars correspond to epicenters of historical and instrumental earthquakes of Mw ≥ 6.0. Fault plane solutions of Mw ≥ 6.0 instrumental earthquakes occurred in the SW Iberian Margin are shown (Fukao, 1973; Buforn et al., 1995, 2004; Stich et al., 2005a, 2005b, 2007). Yellow lines show the active faults (modified from Zitellini et al., 2009; Gràcia et al., 2003a,b; Terrinha et al., 2003). The black outlined box depicts the study area presented in Figure 2. Inset: Setting of the SW Iberia at the boundary between the Eurasian and African Plates.*

2. Regional setting and core site location

The study area is located in the outer Gulf of Cadiz from 34º30'N to 38ºN, in the region between the Gorringe Bank and Portimao Bank, comprising the drainage system and basins from the Tagus Abyssal Plain (TAP), Horseshoe Abyssal Plain (HAP) and NE Seine Abyssal Plain (SAP) (Figs. 1, 2). This region is characterized by an abrupt, irregular physiography dominated by massive ridges and large seamounts, highly incised narrow canyons, and deep, extensive abyssal plains (Fig. 2). The infill of the TAP, HAP and SAP plains is mainly composed by the alternating turbidite and hemipelagic layer composition (Lebreiro et al., 1997; Davies et al., 1997). Lebreiro et al. (1997) also suggested that the emplacement of the Late Quaternary age turbidites, at least for the HAP, was not directly linked to sea-level changes, but probably related to seismic activity. In fact, the most recent turbidite layer identified in the HAP has an emplacement time of 140 ± 120 years BP, coeval with the AD 1755 Lisbon event (Thomson and Weaver, 1994; Lebreiro et al., 1997), suggesting the presence of earthquake-triggered turbidites in the area.

Apart from the abyssal plains, another main study area corresponds to the Infante Don Henrique Basin (IDHB), a slope basin bounded by the foothills of the Gorringe Bank to the west and the Marquês de Pombal Fault (MPF) escarpment to the east (Fig. 2). Associated with active faulting, mass transport deposits have also been recognized in the IDHB at the foot of the Marquês de Pombal fault block (Gràcia et al., 2003a; Vizcaino et al., 2006).

Finally, the drainage pathways to the TAP and HAP have also been sampled for this study to complete the marine synchronicity test and check the confluence channel test in the Gulf of Cadiz. The pathway to the HAP include the Lagos Canyon, Portimao Canyon and southern flank of the Portimao Bank which merge at the Horseshoe Basin, elevated few hundred metres from the HAP.

The first turbidite paleoseismology study in the SW Iberian Margin was carried out by Garcia-Orellana et al. (2006). These authors investigated six short sediment cores (50 cm long) collected by a multicorer in the area stretching from the Tagus to the Horseshoe Abyssal plains for radiometric (^{210}Pb and ^{137}Cs) and sedimentological analyses (Fig. 2). Garcia-Orellana et al. (2006) dated the two recentmost detrital layers and turbidite events (< 150 years), the ages of which correspond to two large (Mw > 6.0) historical and instrumental earthquakes that occurred in the SW Portuguese Margin: the 1909 Benavente and 1969 Horseshoe earthquakes.

2.1. Core site location

This study is based on a total of 21 sediment cores strategically located to characterize the main depositional areas in the SW Iberian Margin (i.e. TAP, HAP, IDHB, SAP) (Table 1). We grouped the sediment cores based on the cruises in which they were sampled:

- **PICABIA-PRIME cruise.** Four giant CALYPSO piston cores, termed MD03 2701 to MD03 2704, were collected during the PICABIA-PRIME cruise (July 2003) on board the French RV Marion Dufresne (Table 1, Fig. 2). Core site MD03 2701 is located in the TAP at 5000 m depth on the NW flank of the Gorringe Bank (Fig. 2). Core site MD03 2702 is located at 3900 m depth in the IDHB, NW of the Marquês de Pombal Fault area. The two last piston cores, MD03 2703 and MD03 2704, were sampled in the HAP around 4800 m depth. They are 12 km apart and separated by an active fault. In addition, four multicores (GeoB 9095-2, GeoB 9005-1, GeoB 9089-1 and GeoB 9099-1) were acquired during the GAP 2003 cruise (RV Sonne) at the same sites as the four CALYPSO piston cores (Fig. 2). These multicores together with multicore MC1 provide information on the uppermost sediment record (Garcia-Orellana et al., 2006), which is often lost during piston coring.

- **SWIM-04 cruise**. Two gravity cores (SW15 and SW18) acquired during the SWIM-04 cruise (August 2004) onboard the Italian RV Urania are included in this study (Table 1, Fig. 2). Core site SW15 was located in the TAP at 5189 m depth, close to the south Gorringe debris avalanche. Core site SW 18 was located at the floor of the Portimao Canyon at 3100 m depth.

- **NEAREST cruise**. Three gravity cores, termed NE01, NE02 and NE03, were acquired during the NEAREST cruise (August 2007) onboard the Italian RV Urania for the paleoseismology study (Table 1, Fig. 2). Core NE01 was acquired on the basin at 3580 m depth, located south if the Portimao Bank. Core site NE02 is located at the mouth of the Sao Vicente Canyon on the HAP (4800 m depth) at the foot of the Horseshoe Fault. Core NE03 was collected at the floor of the Lagos Canyon at 3600 m depth.

- **JC27 cruise**. Twelve piston cores were acquired during the JC27 cruise (August 2008) onboard the British RV James Cook in collaboration with Drs. R. Wynn and D. Masson from the National Oceanography Centre, Southampton (UK) (Table 1, Fig. 2). Core site JC27-20 was located at the NE edge of the SAP at 4287 m. Cores JC27-22#2, JC27-23 and JC27-25 were collected between 4300 and 4600 m deep on the drainage pathway to the HAP. Cores JC27-26, JC27-27, JC27-28 and JC27-30 were acquired at the

NE part of the HAP at around 4800 m depth, and the last two near the mouth of the Sao Vicente Canyon. Cores JC27-31 and JC27-32 were collected at the northern part of the IDHB between 3700 m and 3900 m depth, on the pathway to the TAP. Finally, cores JC27-33 and JC27-34 were sampled at the TAP at more 5000 m depth (Table 1, Fig. 2).

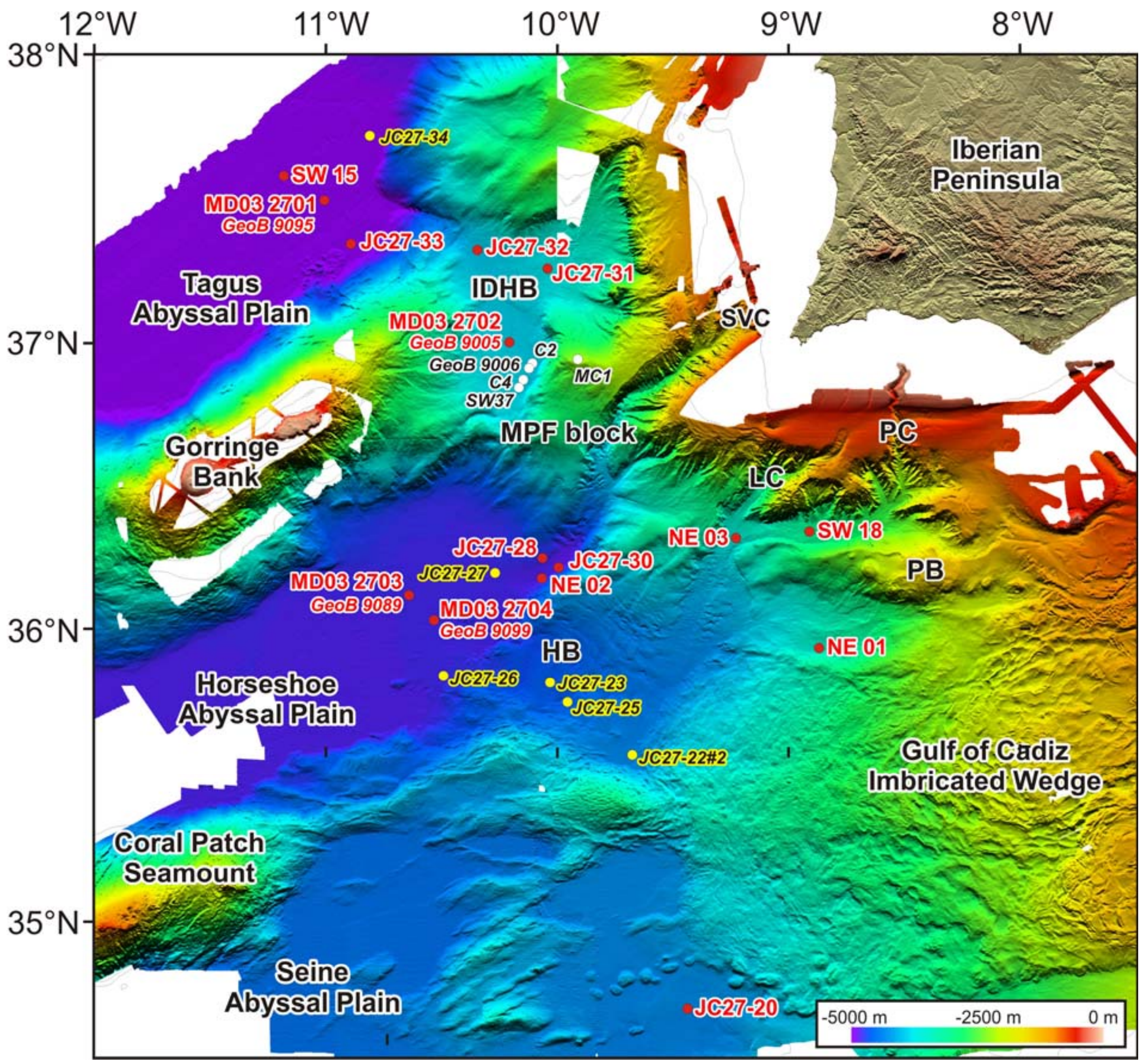

Fig. 2. *Detailed bathymetric map of the external part of the SW Iberian Margin including the Tagus, Horseshoe and NE Seine abyssal plains (ESF EuroMargins SWIM multibeam compilation from Zitellini et al., 2009). Red dots locate the dated sediment cores presented in this report: MD03, GeoB, SW, NE, and selected JC27 cruise cores. GeoB correspond to multicores collected from the same sites as the CALYPSO piston cores (Garcia-Orellana et al., 2006). White dots locate gravity cores in the Marquês de Pombal Fault area (Vizcaino et al., 2006) and multicores MC1 and SW37 (Garcia-Orellana et al., 2006). Yellow dots correspond to the JC27 cruise cores that are analyzed but dating has not been accomplished yet. Their logs are included in Annex I. IDHB: Infante Don Henrique Basin; MPF: Marquês de Pombal Fault; HB: Horseshoe Basin; SVC: São Vicente Canyon; LC: Lagos Canyon; PC: Portimão Canyon; PB: Portimão Bank.*

Table 1. *Characteristics and location of the studied sediment cores.*

Cruise name	Vessel	Year	Gear	Core name	Latitude (°N)	Longitude (°W)	Water depth (m)	Location	Total core length (m)	14C Datings #
PICABIA-PRIME	Marion Dufresne	2003	Giant PC (30 m)	MD03 2701	37°30.01	11°02.01	5052	Tagus Abyssal Plain (TAP)	8.5	7
			Giant PC (30 m)	MD03 2702	37°00.96	10°10.92	3876	Infante Don Henrique Basin	25.5	9
			Giant PC (20 m)	MD03 2703	36°06.27	10°40.09	4807.5	Horseshoe Abyssal Plain (HAP)	19.58	7
			Giant PC (20 m)	MD03 2704	36°02.21	10°34.79	4813	Horseshoe Abyssal Plain	19.31	10
SWIM-04	Urania	2004	GC (10 m)	SW15	37°34.84	11°13.14	5189	Tagus Abyssal Plain	1.17	7
			GC (4 m)	SW18	36°20.27	8°54.97	3131	Portimao Canyon	1.73	3
NEAREST	Urania	2007	GC (4 m)	NE01	35°55.77	8°52.22	3583	South of Portimao Bank	1.67	5
			GC (4 m)	NE02	36°11.31	10°04.47	4800	SVC mouth - Horseshoe Fault	1.75	1
			GC (4 m)	NE03	36°19.34	9°14.41	3600	Lagos Canyon	0.8	1
JC-27	James Cook	2008	PC (12 m)	JC27-20	34°40.0	9°27.45	4285	Seine Abyssal Plain	7.43	4 (in process)
			PC (9 m)	JC27-22#2	35°33.28	9°41.91	4306	Lineation South	5.52	3 (in process)
			PC (9 m)	JC27-23	35°48.07	10°03.35	4614	Horseshoe Basin	5.78	7 (in process)
			PC (9 m)	JC27-25	35°44.75	9°59.27	4635	Horseshoe Basin	6.27	No
			PC (12 m)	JC27-26	35°50.93	10°32.05	4834	HAP	3.36	5 (in process)
			PC (12 m)	JC27-27	36°10.17	10°15.92	4849	NE HAP close to SVC	8.27	3 (in process)
			PC (9 m)	JC27-28	36°14.69	10°3.82	4825	Sao Vicente Canyon Mouth - HAP	5.65	5
			PC (12 m)	JC27-30	36°12.67	10°01.33	4878	Sao Vicente Canyon Mouth- HAP	5.22	4
			PC (12 m)	JC27-31	37°15.73	10°02.84	3787	Infante Don Henrique - HITS Basin	8.23	4
			PC (12 m)	JC27-32	37°18.80	10°21.70	3994	Infante Don Henrique - HITS Basin	9.04	5
			PC (12 m)	JC27-33	37°20.50	10°55.54	5120	Gorringe Bank Landslide - TAP	8.01	4
			PC (12 m)	JC27-34	37°43.09	10°48.89	5066	Eastern margin of TAP	3.71	4 (in process)

2.2. Core quality

Different instruments have been used to sample the sediment cores presented in this report, from giant CALYPSO piston cores, piston cores and gravity cores. The length and quality of the collected sediment sample highly depends on the coring system used.

The CALYPSO piston corer (MD03-2701 to 2704) was designed to acquire very long sedimentary records (> 20 m long). However, the quality of the upper core sections is inhomogeneous owing to piston stretching. For instance, the top of the core may be lost during coring and the upper sections are often deformed showing a bending of laminae in which the apex of bent layer is thickened due to sediment flow (Skinner and McCave, 2003). Bending especially affects the sampling of hemipelagic sediment for dating, which instead of being acquired just below turbidite bases needed to be sampled further downcore (up to 6 cm).

A gravity corer was used to collect NE and SW cores. This gear tends to compress the sedimentary sequence and do not allow to obtain long sedimentary records. With the used (4 m long), the resulting samples are of 1.75 m maximum.

The piston corer was used to collect sediment cores during the JC27 cruise. The used core barrels were 9 and 12 m long, which allowed to obtain cores of slightly more of 9 m long. The cores obtained from this system are the ones of better quality: sedimentary structure was well preserved and no visible deformation was observed.

3. Data and Methods

The methodology followed to study the piston cores included description, imaging, physical properties and geochemical measurements on half core sections. Sediment composition and grain-size analyses, smear-slide description and radiocarbon dating were carried out on selected samples.

3.1. Sediment measurements and analytical procedures

Immediately after core splitting and cleaning, all core sections were imaged with digital colour photo and logged for physical properties at 1 or 2 cm intervals using a multisensor core logger (MSCL) (Fig. 3). These data allowed us to obtain physical properties essential to define the sedimentary facies and the boundaries between turbidite tails and hemipelagites.

Sediment physical property measurements were acquired using different MSCLs. The MD03 cores were measured using the MSCL GEOTEK onboard the RV *Marion Dufresne* which includes magnetic susceptibility, P-wave velocity and gamma-ray attenuation from which density is calculated. The SW and NE cores were measured using the MSCL GEOTEK of the Geotechnical Laboratory of the ICM-CSIC in Barcelona (Spain), which data also included magnetic susceptibility, P-wave velocity, and gamma-ray attenuation. The JC27 cores were measured at the BOSCORF core laboratory at the National Oceanography Centre, Southampton (UK) using the multiple tray (up to seven sections at a time) MSCL GEOTEK which allows to measure magnetic susceptibility together with lightness and colour parameters.

Lightness (L*) and colour parametres (a* and b*) were measured using a spectrophotometer. Detailed core description has been performed based on changes observed in the colour, lithology, texture and structure of the sediments (Fig. 3).

Geochemical composition was measured on archive sections of MD03 cores using the non-destructive X-Ray Fluorescence (XRF) scanner from the University of Bremen (Germany). We measured the following elements: K, Ca, Ti, Fe, Mn, Cu, Sr, V, Cr, Co, Ni, Zn and Pb, at 2 cm interval for cores MD03 2701, MD03 2703 and MD03 2704, and at 1cm resolution for core MD03 2702. The data obtained correspond to the values of element intensity in counts per second (cps), providing information on the relative element concentration. In the present study we selected K, Ca and Ti, which are the elements that better characterize the relationship between detrital and biogenic sedimentation. These data help us to characterize different types of turbidites as well as to define the hemipelagic intervals between turbidites that are essential to calculate the age models. Calcium carbonate content analyses were performed on SW, NE and JC27 cores by the leaching acid method using a Bernard calcimeter of the ICM-CSIC Laboratory in Barcelona (Spain). The results are expressed as % of equivalent $CaCO_3$ weight.

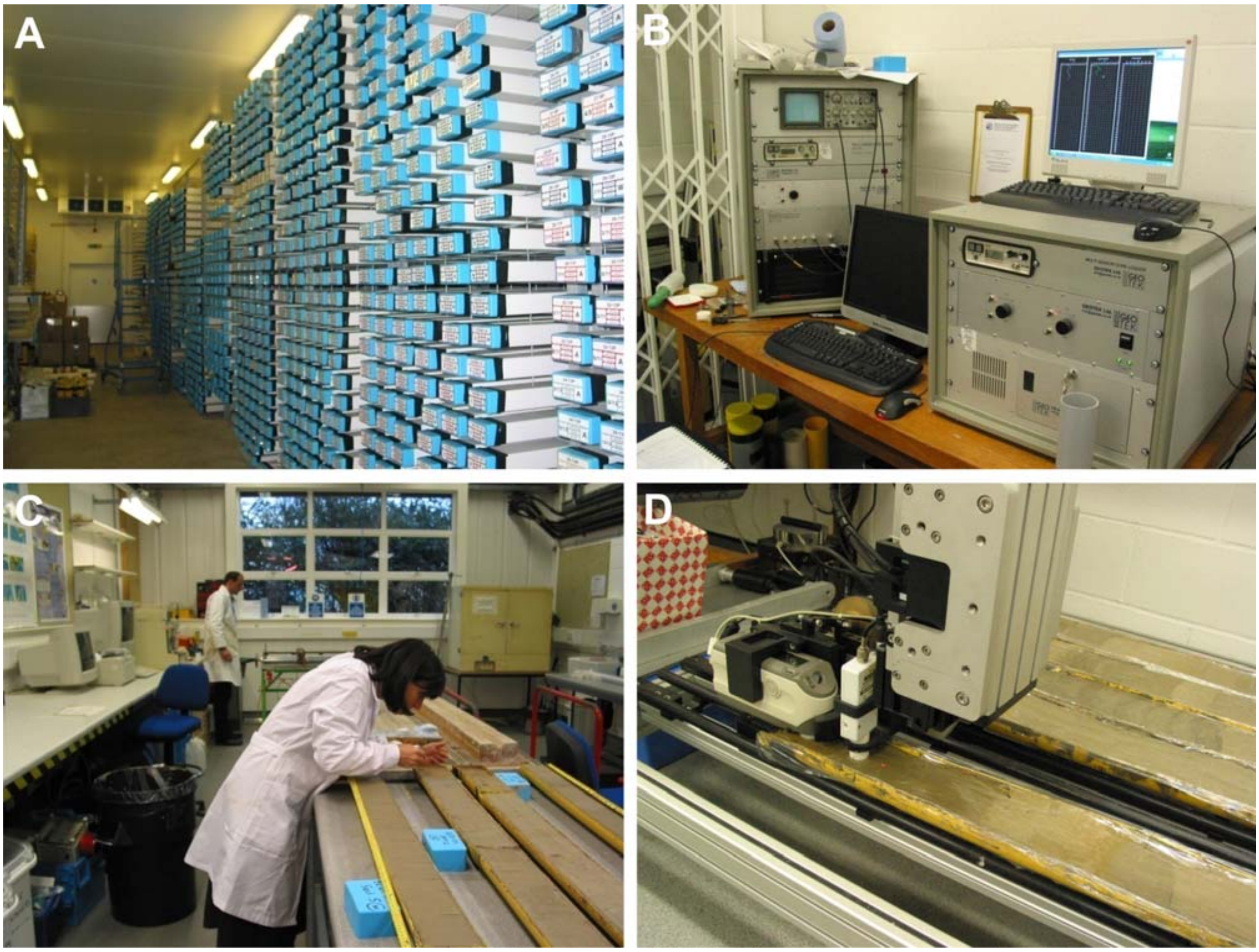

Fig. 3. *A: BOSCORF core repository (NOCS, UK). B: GEOTEK acquisition system. C: Core sampling at the BOSCORF laboratory. D: Logging lightness and magnetic susceptibility using the GEOTEK multiple tray multi-sensor core-logger.*

Grain-size analyses were systematically carried out every 10 cm and with a higher resolution sampling (2 cm) on turbidites bases and tails intervals. The exception was in the homogeneous core MD03 2702 with a sample interval of 20 cm. A total of 205 samples were analyzed for the MD03 cores, 120 samples for the SW and NE cores, and 872 samples for the JC27 cores. We used the Coulter LS200 from the *GRC Geociències Marines* group of the University of Barcelona, which provides the grain-size data as a volume percentage for all the textural distribution (< 4 μm to 2 mm). Texture parameters were also obtained (grain-size distribution, mean grain-size, standard deviation, kurtosis, etc). Sand fraction and very coarse silt components (> 50 μm) were identified using a binocular microscope. Relative mineral abundance was estimated by counting a minimum of 300 grains per sample. In addition, to define the boundary depths between turbidite tails and hemipelagites, 150 smear slides were qualitatively analyzed.

3.2. Radiocarbon dating, calibration and age models

Radiocarbon dating was performed using samples of hemipelagic sediment mainly located about 0.5 to 2 cm below the turbidite bases, locally reaching up to 6 cm in some samples of the MD03 cores. For ^{14}C AMS dating, A. Asioli (CNR-Padova) was in charge of checking and preparing the samples, and hand-picking between 7 and 10 mg individual foraminifera of the same species with a diameter larger than 250 μm. Orbulina universa was preferentially used because it was the most common species, although we also selected Globorotalia inflata, Globigerinoides ruber (var. *alba*), Globigerinoides sacculifer; Globigerinoides conglobatus, Neogloboquadrina pachyderma, and mixed samples. Foraminifera were prepared and dated at the National Ocean Sciences Accelerator Mass Spectrometry Facility (NOSAMS-WHOI laboratory, Woods Hole, USA). Finally, a total of 63 samples have been already dated: 24 for the MD03, 10 for the SW cores, 7 for the NE cores, 22 for JC27 cores (Table 2). In addition, 26 additional samples of JC27 cores are being processed at NOSAMS-WHOI laboratory for ^{14}C AMS dating (Table 1) and we expect to have the ages by end of April 2010.

To obtain an accurate turbidite event chronology, the first step was to calibrate the ^{14}C ages of the hemipelagic sediment samples using the Marine0.9 curve (Reimer et al., 2009) included in the Calib 6.0 software. To this end, it is necessary to know the value of ΔR, the site-specific offset from the global ocean reservoir. In the SW Portuguese Margin, ^{14}C dating of marine shells and associated charcoal or bones from archaeological sites with ages spanning the Holocene yielded a wide range of reservoir ages suggesting fluctuations in the intensity of coastal upwelling (e.g. Monge Soares and Alveirinho Dias, 2006). However, most of the values obtained for the Holocene period are lower than the modern value (250 ± 25 ^{14}C yr). To find a suitable ΔR value, we considered the weighted mean of the ΔR obtained for the period from 3000 to ~ 600 yr BP, which was sampled at a greater resolution including more than 30 ΔR values. This period, with a weighted mean of 95 ± 15 ^{14}C yr, seems to have lower upwelling than at present (Monge Soares and Alveirinho Dias, 2006). The resulting calibrated ages using this ΔR are given in Table 2.

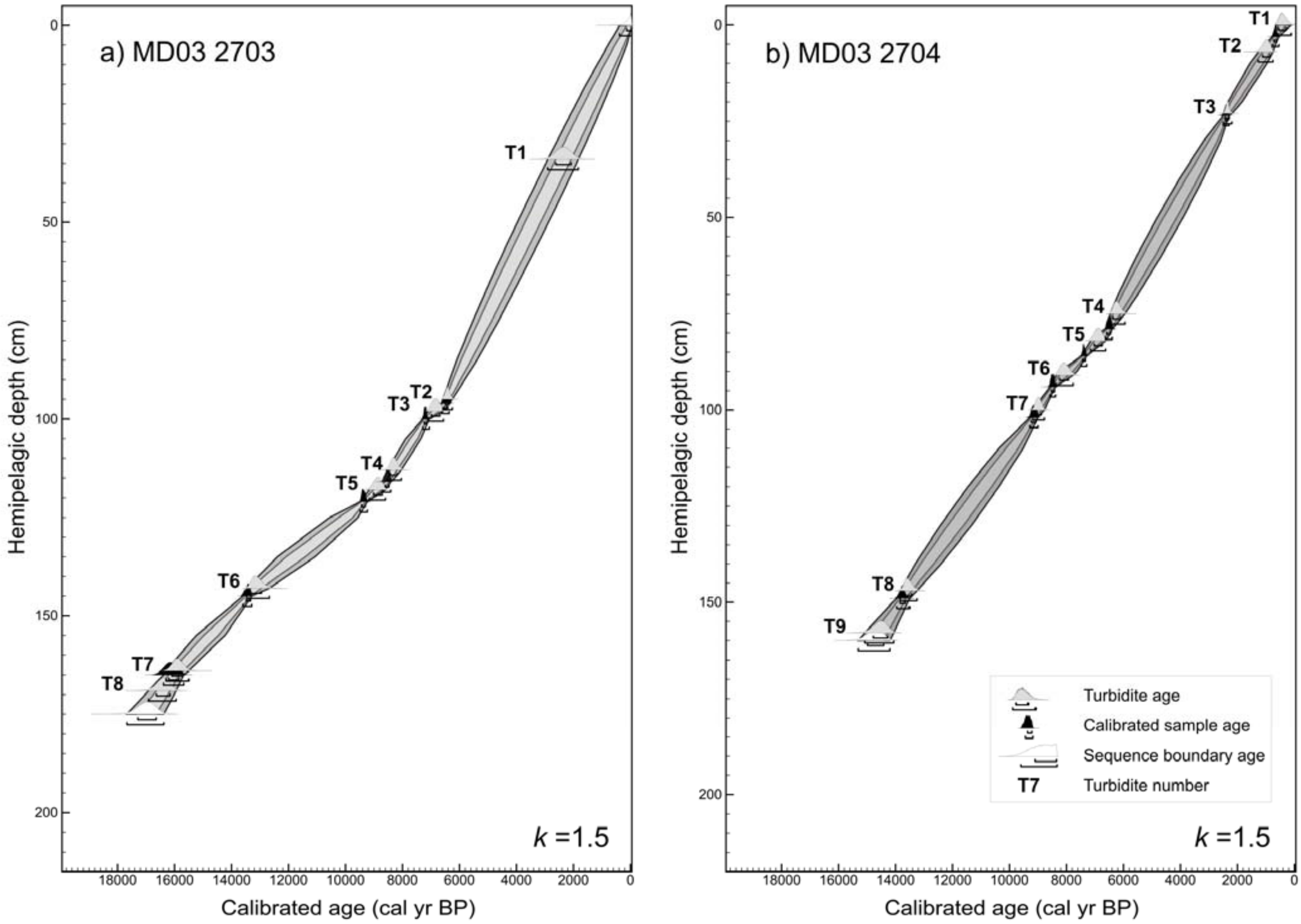

Fig. 4. *Age-depth model output for cores MD03-2703, and MD03-2704 assuming the deposition is a Poisson process using P_Sequence from OxCal 4.0 software (Bronk-Ramsey, 2008). 1σ and 2σ probability distributions are depicted for the calibrated sample ages (in black), sequence boundary ages (in white) and modelled turbidite ages (in grey). The value of k used to run each age model is indicated.*

In the case of the MD03 cores, the next step was to determine the age of each single turbidite with sufficient precision and accuracy. Since the samples of hemipelagic sediment on MD03 cores are located a few cm below the base of the turbidites or tens of cm above the turbidite tails, it was necessary to interpolate or extrapolate the ages of the calibrated samples as far as the base or top of the neighbouring turbidite intervals. For this purpose we used the P_Sequence, a Bayesian model of deposition implemented in the computer program OxCal 4.0 (Bronk Ramsey, 2008). Given that the hemipelagic sedimentation rate cannot be regarded as perfectly constant, the P_Sequence depositional model takes into account the uncertainties in the variation of the hemipelagic sedimentation rate by regarding sedimentation as an inherently random process. The resulting age model, referring to the calibrated age scale, reflects the increasing uncertainties with distance from the calibrated sample ages (Fig. 4).

To run the P_Sequence model, apart from the ΔR, several input parameters are needed. First, the uncalibrated ^{14}C ages and their corresponding sample depths are provided as the main dataset. Second, the uncalibrated ages of the top and bottom boundaries of each core are estimated. These are determined with ample margins, only constrained by the age of the seafloor at the time of sampling and by the age of the shallowest sample for top boundaries, and by the age of the deepest sample for bottom boundaries. Finally, the regularity of the sedimentation process is determined by factor k, with the higher values of k reflecting smaller variations in sedimentation rate (Bronk Ramsey, 2008). For each core, we chose the highest possible values of k, on condition that the modelled age fitted each individual calibrated age with $\chi^2 < 1$ (all agreements > 68.2% in P_Sequence model output). Applying this criterion, we used k=1.5 for cores MD03 2703 and MD03 2704, and k=1 and k=0.8 for cores MD03 2701 and MD03 2702, respectively. For each core we obtained the 68% and 95% probability ranges which are plotted in the calibrated age vs. hemipelagic depth model (Fig. 4). Based on the hemipelagic depth of every single turbidite, the age models yield the calibrated ages which are reported as maximum probability values, 1σ and 2σ age ranges in Table 2. In the following sections, turbidite calibrated ages are reported with 1σ ranges based on the most likely turbidite correlations that characterize the occurrence of events.

Owing to the limited number of cores available for this study, it was not possible to quantify basal erosion in the calculation of the time interval between the dated sample and the turbidite base (e.g. Nelson et al., 1996; Gutiérrez-Pastor et al., 2009). Consequently, turbidite erosion was assumed to be negligible for modelling the ^{14}C dates to obtain the ages of the turbidites.

Table 2. *AMS ^{14}C data and sample age calibrations of the studied cores.*

Core #	AMS lab reference	Core depth (cm)	Foraminifera sampled	Radiocarbon age (yr BP ± 1σ)	ΔR (*)	1σ calibrated age (Cal yr BP)	Area prob. dist. (1σ)	2σ calibrated age (Cal yr BP)	Area prob. dist. (2σ)
MD03 2701	49063	25-27	Mixed	2530±100	95±15	1940 - 2210	1	1850 - 2320	1
	49064	65-67	*Orbulina universa, G. sac.*	5200±70	95±15	5395 - 5565	1	5300 - 5590	1
	49065	130-132	*Orbulina universa*	6770±40	95±15	7160 - 7250	1	7110 - 7310	1
	49066	218-220	*Orbulina universa*	8650±60	95±15	9100 - 9290	1	9020 - 9375	1
	52940	230-232	Mixed	8760±55	95±15	9275 - 9415	1	9180 - 9470	1
	49067	289-291	*Globigerinoides ruber*	9700±45	95±15	10425 - 10535	1	10340 - 10570	1
	49068	370-372	*Orbulina universa*	12100±60	95±15	13350 - 13505	0.987	13290 - 13635	1
MD03 2702	49069	56-57	*Orbulina universa, G. rub.*	(6500±130)[a]	--	--	--	--	--
	52124	80-81	*Orbulina universa, G. rub.*	1230±45	95±15	645 - 725	1	610 - 790	1
	49070	235-237	*Orbulina universa*	7840±50	95±15	8160 - 8285	1	8085 - 8340	0.994
MD03 2703	49077	42-44	Mixed	(1870±35)[b]	--	--	--	--	--
	49078	168-172	*Globigerinoides ruber*	6100±45	95±15	6355 - 6480	1	6295 - 6540	1
	49079	185-187	*Globigerinoides ruber*	6770±40	95±15	7160 - 7250	1	7110 - 7310	1
	49080	225-227	*Orbulina universa, G. con.*	8150±50	95±15	8445 - 8570	1	8385 - 8635	1
	49081	259-261	*Orbulina universa*	8790±55	95±15	9305 - 9440	1	9230 - 9490	1
	49082	348-350	*Orbulina universa*	12100±60	95±15	13350 - 13505	0.987	13290 - 13635	1
	49083	438-440	*Neogloboquadrina pachyderma*	14100±70	95±15	16670 - 16865	1	16505 - 16960	1
MD03 2704	49084	50-52	Mixed	1200±60	95±15	615 - 725	1	545 - 775	1
	52122	103-104	*Orbulina universa, G. sac.*	2790±35	95±15	2330 - 2435	1	2280 - 2530	1
	49085	216-218	*Orbulina universa, G. rub.*	6150±45	95±15	6405 - 6535	1	6360 - 6615	1
	49086	236-238	*Globigerinoides ruber*	6970±45	95±15	7335 - 7430	1	7285 - 7480	1
	49087	284-286	*Globigerinoides ruber*	8140±45	95±15	8435 - 8555	1	8390 - 8605	1
	49088	325-327	*Orbulina universa*	8600±55	95±15	9050 - 9220	0.981	8985 - 9290	1
	49089	507-509	*Orbulina universa, G. rub.*	12400±85	95±15	13665 - 13850			
SWIM 15	69674	0-2	Mixed	1390±20	95±15	800 - 885	1	765 - 910	1
	69675	6 - 8	*Globorotalia inflata*	2410±20	95±15	1885 - 1965	1	1850 - 2010	1
	69676	27 - 29	Mixed	4890±20	95±15	4990 - 5135	0.968	4955 - 5215	1
	69677	45.5 - 47.5	*Globorotalia inflata*	6690±35	95±15	7055 - 7180	1	7000 - 7225	1
	69678	57 - 59	*Globorotalia inflata*	7530±30	95±15	7860 - 7935	1	7815 - 7970	1
	69679	85.5 - 87	Mixed	9790±40	95±15	10515 - 10585	1	10475 - 10655	1
	69680	112	Charcoal	18050±90[c]	--	21350 - 21665	1	21255 - 22000	1
SWIM 18	69681	2 - 4	Mixed	>Mod	95±15	> 1950 AD			
	69682	42 - 44	*Globorotalia inflata*	3040±20	95±15	2705 - 2745	1	2675 - 2775	1
	69683	72 - 74	Mixed	4120±25	95±15	3980 - 4085	1	3930 - 4145	1
NE01	69667	0-2	Mixed	1240±20	95±15	660 - 715	1	645 - 750	1
	69668	16-18	Mixed	3000±20	95±15	2675 - 2725	1	2605 - 2745	1
	69669	34-36	Mixed	5050±20	95±15	5260 - 5320	1	5240 - 5415	1
	69670	69-71	*Orbulina Universa*	12000±45	95±15	13295 - 13400	1	13245 - 13465	1
	69671	79-81	*Globorotalia inflata*	12850±55	95±15	14115 - 14540	1	14040 - 14895	1
NE02	69672	1-3	Mixed	300±25	95±15	26-48	1	*Invalid age* for this cal. curve	
NE03	69673	0.5-2.5	Mixed	905±20	95±15	430 - 480	1	395 - 505	1
JC27-28	75535	7-9	*Globorotalia inflata*	1490±30	95±15	900 - 975	1	870 - 1045	1
	75536	28-30	*Globorotalia inflata*	3820±35	95±15	3580 - 3695	1	3540 - 3795	1
	75537	116-118	*Globorotalia inflata*	5750±35	95±15	5990 - 6115	1	5945 - 6170	1
	75538	225-227	*Globorotalia inflata*	11000±50	95±15	12360 - 12425	0.364	12240 - 12590	1
						12430 - 12545	0.636		
	75539	384-386	*Globorotalia inflata*	19200±75	95±15	22215 - 22420	1	22090 - 22505	1
JC27-30	75540	8-10	Mixed	2090±30	95±15	1510 - 1605	1	1460 - 1675	1
	75541	56-58	*Globorotalia inflata*	2380±25	95±15	1855 - 1940	1	1815 - 1980	1
	75542	234-236	*Globorotalia inflata*	9560±40	95±15	10240 - 10365	1	10205 - 10440	1
	75543	407-409	*Globorotalia inflata*	19350±75	95±15	22290 - 22530	1	22190 - 22675	0.907
JC27-31	75526	67-69	*Globorotalia inflata*	3800±20	95±15	3580 - 3665	1	3535 - 3710	1
	75527	174-176	*Globorotalia inflata*	9450±50	95±15	10150 - 10240	1	10095 - 10360	1
	75528	436-438	*Globorotalia inflata*	16550±50	95±15	18980 - 19125	0.44	18930 - 19415	1
						19240 - 19405	0.56		
	75529	558-560	Mixed	19550±100	95±15	22430 - 22710	0.645	22345 - 23035	0.857
						22745 - 22955	0.355	23070 - 23290	0.143
JC27-32	75530	5-7	*Globorotalia inflata*	1050±25	95±15	515 - 565	0.872	500 - 620	1
						580 - 595	0.128		
	75531	305-307	*Globorotalia inflata*	19300±80	95±15	22270 - 22490	1	22140 - 22655	0.96
	75532	351-353	*Globorotalia inflata*	25100±110	95±15	29330 - 29555	1	29120 - 29820	1
	75533	541-543	*Globorotalia inflata*	30400±180	95±15	34520 - 34790	1	34405 - 34975	0.904
	75534	663-665	Mixed	32700±230	95±15	36485 - 36875	1	36295 - 37380	1
JC27-33	75544	14-16	*Globorotalia inflata*	5590±40	95±15	5825 - 5935	0.982	5745 - 5975	1
	75545	56-58	*Globorotalia inflata*	8700±40	95±15	9215 - 9360	1	9125 - 9400	1
	75546	307-309	Mixed	18650±100	95±15	21455 - 21875	1	21365 - 22100	1
	75547	612-613	Mixed	22700±230	95±15	26185 - 27010	0.978	26050 - 27660	1

* Local reservoir correction (ΔR) for the Portuguese margin based on Monge Soares and Alveirinho Dias (2006).
Ages in brackets are not used in the present study: a) Sample obtained within a debrite; b) Sample rejuvenated by mixing from overlying sediment.
c) This sample age has been calibrated using the IntCal09 calibration curve
G. sac.: Globigerinoides sacculifer; G. rub.: Globigerinoides ruber; G. con.: Globigerinoides conglobatus.

4. Sedimentary facies

Based on grain-size analyses, three main sedimentary facies were distinguished in the studied cores: 1) hemipelagites, 2) debrites and 3) turbidites.

Hemipelagite facies was mainly described as homogeneous olive (Munsell notation 5Y 5/4) bioclastic silty-clay (52.4 % clay, 43.6 % silt and 3.9 % sand and a mean diameter of 6.2 Φ). Hemipelagites are commonly highly bioturbated. The thickness of hemipelagic deposits ranges from few millimetres up to 60 cm, with exception of core MD03 2702, where a single hemipelagic interval exceeds 220 cm in thickness.

Debrite facies characterized by homogeneous greyish brown silty-clay (46.7 % clay, 48.1 % silt and 5.2 % sand and a mean diameter of 6.2 Φ). Despite textural similarities with hemipelagite, debrite tends to be darker (brownish) with an absence of bioturbation. It is commonly characterized by the presence of colour patches which corresponds to mud clasts and soft sediment deformation structures.

Turbidite facies are characterized by sharp and erosional bases, fining upward sequences and, commonly, internal sedimentary structures (such as parallel and cross lamination). Turbidite bases present a coarse interval with about 18.7 % clay, 30.8 % silt and 50.5 % sand and mean diameter of 2.5 Φ. Turbidite tails are characterized by modal grainsize distribution composed by an average of 48.5 % clay, 51.3 % silt and 0.2 % sand and mean diameter of 6.5 Φ. Both represent well-distinguished sedimentary layers described in the Bouma sequence.

5. Texture, Physical properties, Geochemistry and Chronology of turbidite deposits

In this section we present the texture, physical properties, geochemistry and chronology of the sedimentary facies identified on the studied cores (Table 2). The data is presented by each of the study areas: Tagus Abyssal Plain (TAP), Infante Don Henrique Basin (IDHB), drainage pathways to the HAP, Horseshoe Abyssal Plain (HAP), and Seine Abyssal Plain (SAP). In Annex I are included the logs of the JC27 sediment cores that have been analyzed but which dating results are not available yet.

Downcore variability of the magnetic susceptibility (MS), density and lightness (L*) allowed us to complete a detailed characterization of the sedimentary facies. Geochemistry data allows us to recognize relative abundances of terrigenous and biogenic sediment supply, based on the variability of K/Ti (detrital proxy) and Ca/Ti (biogenic calcareous proxy) ratios.

5.1. Tagus Abyssal Plain

Four sediment cores collected in Tagus Abyssal Plain (MD03 2701, SW15, JC27-33 and JC27-34) have been analyzed and dated (Fig. 2). In this section, we focused on MD03 2701 and SW15, which are the cores that better reflect the basin infill. Core JC27-33 is the core closer to the North Gorringe debris avalanche and JC27-34 is located at the foot of the Sines Spur. The logs of both cores (JC27-33 and JC27-34) are included in Annex I.

Core MD03 2701 is composed by hemipelagites interlayered between 8 turbidite intervals. Hemipelagites are characterized by low MS values (around 10 SI) and density values of about 1.9 gr/cm^3. They are characterized by K/Ti measurements varying from 1.5 up to 2.5 and Ca/Ti from 10 to 35 (Fig. 5).

Turbidite layers (T1 to T8) are grey to olive grey (5Y 5/1 to 5Y 4/2) with a thickness ranging from 3 to 60 cm (Fig. 5). The sand fraction is composed of quartz, feldspar, carbonates, micas and biogenic components (mainly foraminifera) reaching 45% of the total of this fraction. Turbidites were classified as poorly sorted sand to silt with a mean diameter of 1.9 Φ (T7) to 5.4 Φ (T6) (Fig. 5). However, two silty-clay turbidites (mean diameter of 6.7 Φ) were identified in the upper section (T1 and T3). Few sand layers showing a disrupted sedimentary structure appear anomalously intercalated in the sedimentary sequence from the sides of the core (Fig. 5). They resulted from disturbance during piston coring. However, it was possible to accurately identify these artefacts and exclude them from the dataset.

In core MD03 2701 turbidites were divided into two groups based on MS and density. The first group corresponds to the turbidite deposits from T1 to T6, with MS ranging between 9 and 14 SI and density from 1.8 to 2.0 gr/cm^3. The second group including T7 and T8 presents higher MS values reaching up to 40 SI whereas density ranges from 1.9 to 2.4 gr/cm^3 (Fig. 5). Turbidite layers are darker (L* = 42) than the hemipelagites (L* = 55). This suggests that the lightness shows a good correspondence with the sediment composition and texture. Turbidites are characterized by K/Ti measurements ranging between 1.5 and 3 whereas Ca/Ti is roughly constant (13), locally increasing up to 20 in T8 (Fig. 5).

The 6 uppermost turbidites (T1, T2, T3, T4, T5 and T6) recorded in core MD03 2701 were deposited during the Holocene at around 1980 – 2280 yr BP, 4960 – 5510 yr BP, 7105 – 7250 yr BP, 8540 – 8985 yr BP, 9230 – 9370 yr BP, 10175 – 10425 yr BP, respectively (Table 2). The remaining two turbidites (T7 and T8) occurred during the Last Glacial-Interglacial Transition period at around 13310 – 13515 yr BP and 15020 – 16630 yr BP, respectively (Table 2).

Core SW15 is a short core (1.25 m) characterized by relatively thin (10-15 cm) hemipelagic intervals between turbidite layers. Hemipelagites are light olive brown (2.5Y 5/4) to olive (5Y 4/3), homogeneous structureless mud. In some intervals millimetre-thick oxidation layers and sulphide mottles are observed. Hemipelagic intervals clearly show high lightness values (50) which are correlated with high $CaC0_3$ content.

A thick sequence of 6 fine-grained turbidites (T1 to T6), some with sandy bases have been identified. The two upper turbidites (T1 and T2) show olive (5Y 4/3) well sorted very fine sand at its bases. Bases are sharp, irregular and erosive. Turbidite tails are silty clays showing with light olive brown (2.5Y5/3) mottles and oxidation laminae. Structures of parallel lamination are observed. Downcore, subsequent turbidite intervals T3/T4 and T5/T6 are separated by a thin hemipelagic interval. T3 and T5 show thick (10-15 cm) olive grey (5Y 4/2) to dark grey (5Y 4/1) very fine to fine sand bases which probably eroded the tails of T4 and T6, respectively. Black spots of organic matter and cross lamination are observed. Physical properties increase downcore. High MS values (30) are measured at the base of T6. Density and P-wave velocity reach its highest measured values (1.85 gr/cm^3 and 1700 m/s, respectively) at the bases of turbidites T3 to T6. Low values of total carbonate (12-14 wt%) are measured at the turbidite bases in correspondence with the lowest values around 30 (darker colours) in lightness.

Regarding the chronology, ^{14}C ages have been obtained for both the hemipelagic intervals immediately at the top and at the base of turbidites. As the ages obtained below turbidites bases are much older that the ones obtained at the top of the turbidite tails, it suggests these turbidites have an important erosive potential. The 4 first turbidites recorded in core SW15 were deposited during the Holocene at around 1885 - 1965 yr BP (T1), 4990 - 5135 yr BP (T2), 7860 - 7935 yr BP (T3), 10515 - 10585 yr BP (T4). The remaining two turbidites (T5/T6) occurred during the Last Glacial-Interglacial Transition period between 10515 - 10585 and 21350 - 21665 (Table 2).

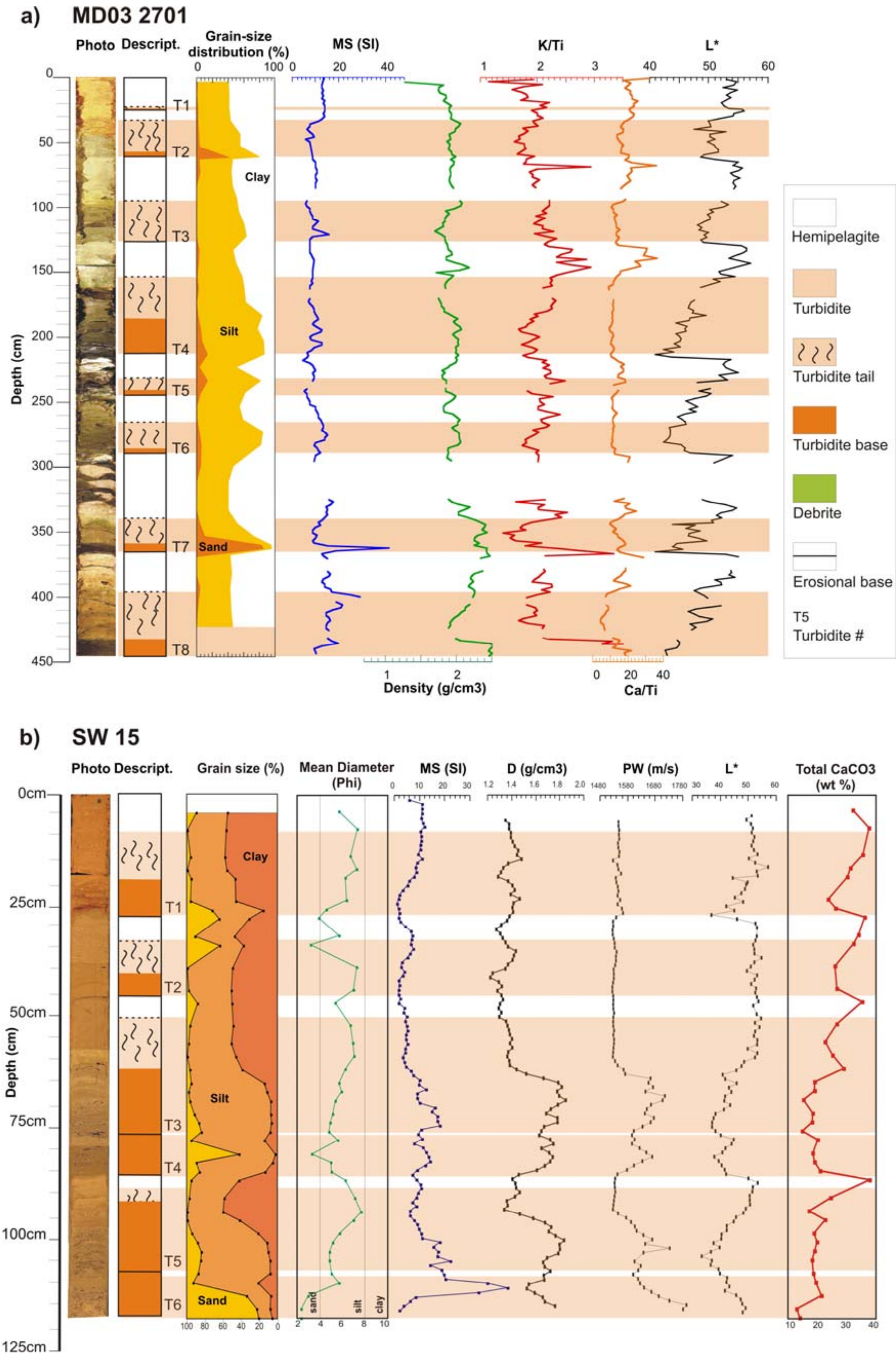

Fig. 5. *Image, lithological description, grain-size distribution, magnetic susceptibility, density and geochemical composition of the studied sections of the core MD03 2701 and core SW 15 from the Tagus Abyssal Plain. Turbidite numbers are depicted for each core.*

5.2. Infante Don Henrique Basin

Three sediment cores, MD03 2702, JC27-30 and JC27-31, were collected in the Infante Don Henrique slope basin (IDHB) and have been analyzed and dated (Fig. 2). Cores JC27-30 and JC27-31 were collected in the northern sub-basin floor, at the gather zone prior to plunging down the slope to the Tagus Abyssal Plain. In this section, we present the results of cores on MD03 2701 and it nearest core JC27-30. The log of core JC27-31 is included in Annex I.

In core MD03 2702 (IDHB), 2 turbidites (T1 and T2), 30 and 25 cm thick respectively, are characterized as greyish brown (2.5Y 5/2) sandy silt. These two turbidites are mainly composed of biogenic compounds. A debrite was identified under turbidite T1 between 51 and 66 cm depth (Fig. 6). Hemipelagites, debrites and turbidites facies show fairly constant MS values (8 to 18 SI). This is not the case for density and L*, which increase from 1.5 to 2.4 gr/cm^3 and from 45 to 53, respectively (Fig. 6). The uppermost turbidite (T1) and debrite could not be geochemically analyzed because of the watery conditions of the sediment that were unsuitable for XRF scanning. In general, K/Ti and Ca/Ti do not show large oscillations in core MD03 2702 (Fig. 6). In turbidite T2, the detrital ratio was lower than expected with values reaching 1.5 whereas the calcareous ratio ranged between 14 and 26. This might be explained by the relative abundance of transported biogenic components (mainly foraminifera) with respect to siliciclastic components. Hemipelagites shows K/Ti values of 1.7 to 2.9 and of Ca/Ti between 10 and 36. The uppermost turbidite (T1) and debrite was deposited at around 385 – 545 yr BP while turbidite (T2) was deposited at 7880 – 8145 yr BP (Table 2).

Core JC27-30 is characterized by a thick sequence of apparently hemipelagic muds with one muddy sand debris flow unit towards the bottom of the core (Fig. 6). Hemipelagite are homogeneous light olive grey to grey bioturbated mud (mean diametre of 7 Φ) with scattered foraminifera. In some sections black sulfide rings/pockets are observed. MS and lightness values are relatively constant, with values of 15-25 SI and 45-50, respectively. Total carbonate ranges between 20 and 30 wt% all along the core. Between 610-695 cm below seafloor, a debrite has been identified (Fig. 6). The debrite is composed of grey mud to grey highly bioturbated silty mud with black silty layers. Grey brown very fine sand containing quartz, lithics and foraminifera are located at the base, with a mean diametre of 4 Φ. MS values are relatively higher (around 30) than the rest of the core, whereas lightness show slightly darker values (45). At 690 cm, carbonate maximum (47 wt%) correlates with the sandy base of the debrite, rich in foraminifera. Four ages have been obtained, denoting a low sedimentation rate (Table 2). Ages of 3580 - 3665 yr BP at 67-69 cm and 10150 - 10240 yr BP at 174-176 cm have been obtained for the Holocene section. The debrite has an age older than 23000 yr BP, around the Last Glacial Maximum.

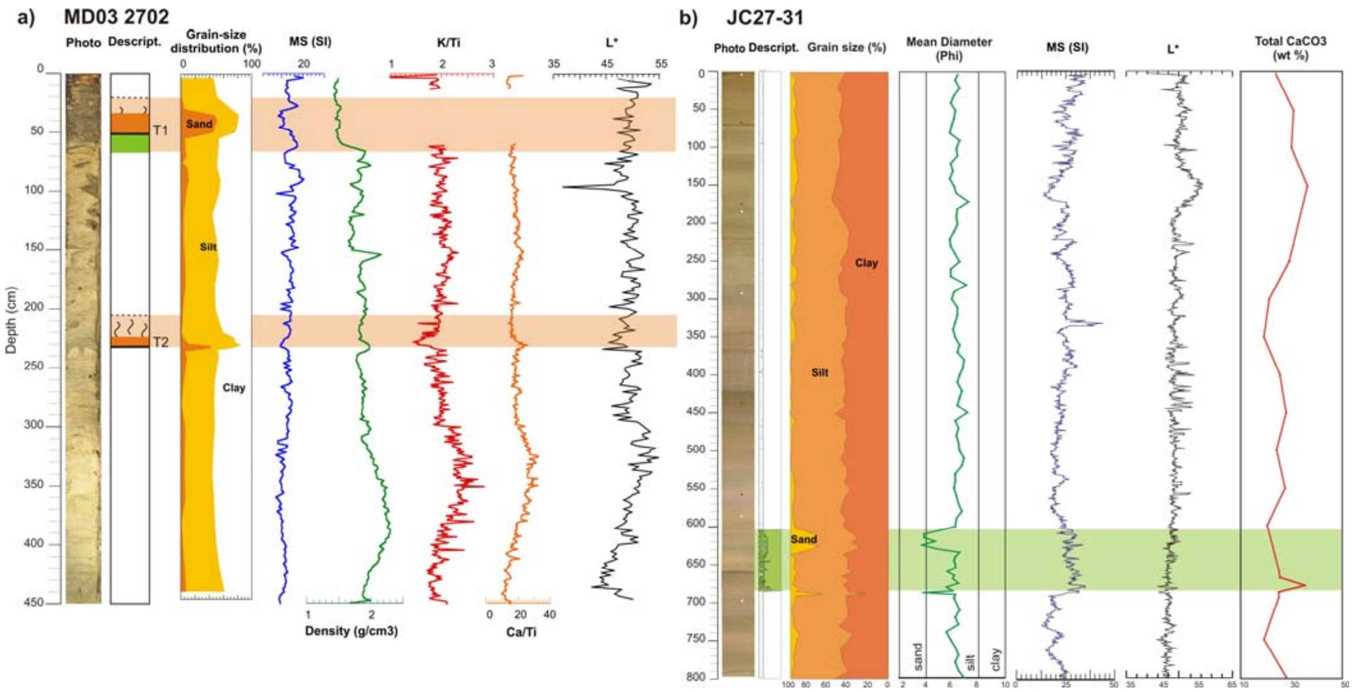

Fig. 6. *Image, lithological description, grain-size distribution, magnetic susceptibility, density and geochemical composition of the studied sections of the core MD03 2702 and core JC27-31 from Infante Don Henrique Basin. Turbidite numbers are depicted. See caption in Figure 5.*

5.3. Drainage pathways to HAP: Portimao and Lagos Canyon and Horseshoe Basin

Six sediment cores (SW18, NE01, NE03, JC27-22, JC27-23 and JC27-25) were collected downstream from the Portimao, Lagos Canyon and Horseshoe Basin along the sediment pathways draining to the Horseshoe Abyssal Plain (Fig. 2). In this section, we focus on SW18, upstream from NE03, which is located on the pathway from the Portimao and Lagos Canyons, and NE01, located on the south flank of the Portimao Bank, on the bypass area at the front of the imbricated wedge. Cores JC27-22, JC27-23 and JC27-25 are located on the Horseshoe Basin, but radiocarbon dating is not available yet. The logs of these cores are included in Annex I.

The cores were dominated by thick sand-mud turbidites and a low proportion of hemipelagite indicated a fairly rapid accumulation rate. Core SW18 was composed of three turbidites and a debrite. Hemipelagites are olive brown (2.5Y 4/3), light olive brown (2.5Y 5/3) to olive grey (5Y 4/2) homogeneous and structureless mud. Turbidite bases are dark grey (5Y 4/1) fine to medium sand slightly parallel laminated, mostly of detrital composition (30% biogenic, 70% minerals), with irregular, erosive bases. They show a fining upward sequence to dark grey (5Y 4/1) fine to very fine sand, sometimes showing oblique lamination. Turbidite tails are olive (5Y4 /3) mottled mud to clayed silt. Turbidites are characterized by values of MS from 10 to 15 SI, density from 1.4 to 1.7 gr/cm^3, P-wave velocity around 1520 m/s, and lightness about 42 (Fig. 7). A thick > 85 cm thick, debris flow deposit is observed at the base of the core. It is composed of a olive grey (5Y 4/2) heterogeneous interval made of irregular silty clay and clayed silt pockets. Mud clasts of different size show internal lamination and highly dipping layers. Abundant black (5Y 2.5/1) spots of organic matter are also observed. Towards the bottom of the interval, intensive soft sediment deformation is observed with elongated, folded bands and large (few cm thick) banded clasts. Regarding physical properties, the debris flow show higher values in density (1.8 gr/cm^3) and lower values (35) in lightness (Fig. 7). The top of the core (2-4 cm) is very recent (> 1950 AD), denoting that the recent most sedimentary layers have been preserved during coring. The uppermost turbidite (T1) has an age younger that 2705 - 2745 yr BP while turbidite (T2) was deposited between 2705 - 2745 yr BP and 3980 - 4085 yr BP. T3 and the debrite are older that 3980 - 4085 yr BP (Table 2).

Core NE01 is composed by a sequence of 2 thick sand-mud turbidites with well-developed bases. Hemipelagic intervals are found at the very top of the core and in a 25 cm thick layer between the two turbidites (Fig. 7). Hemipelagites are light olive brown (2.5Y 5/4) to olive brown (2.5Y 4/3), homogeneous mud to silty clay with organic-rich dark mottles. No internal structures are observed. Turbidite T1 show a thick sandy base and thin mud cap. It shows a sharp, erosive, irregular base with a fining upward sequence, ranging from medium sand to silt (from 3 Φ to 6 Φ). T2 shows a very thick turbidite tail. It is dominated by a light olive brown (2.5Y 5/3) mottled mud with scattered shell fragments. Its lower interval is composed by fine sand pockets. Turbidites are characterized by relatively constant values of MS (around 12 SI), density (1.3 gr/cm^3) and P-wave (1500 m/s) locally increasing to 27 SI, 1,.8 gr/cm^3 and 1680 m/s at turbidite bases. Lightness and total calcium carbonate are variable downcore, ranging from *L 40 to 50 and 20-30 wt%, respectively (Fig. 7). The uppermost turbidite (T1) has an age between 660 - 715 yr BP and 2675 - 2725 yr BP, whereas T2 has an age older than 5260 - 5320 and younger than 13295 - 13400 yr BP (Table 2).

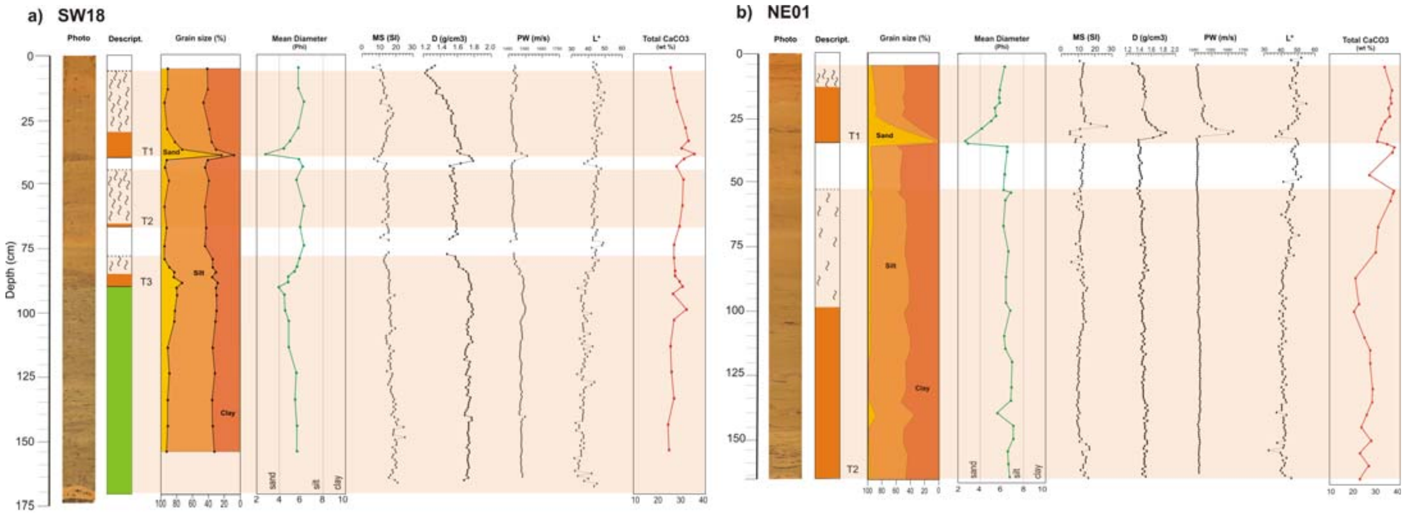

Fig. 7. *Image, lithological description, grain-size distribution, physical properties and total carbonate composition of core SW18 and NE01 located along the drainage pathways to the HAP. Turbidite numbers are depicted. See caption in Figure 5.*

5.4. Horseshoe Abyssal Plain

Seven sediment cores were collected in the Horseshoe Abyssal Plain (MD03 2703, MD03 2704, NE02, JC27-26, JC27-27, JC27-28 and JC27-30) have been analyzed and some of them dated (Fig. 2). In this section, we focused on MD03 2704, which is similar to MD03 2703 although it has a more complete record, and JC27-30 on the northern levee of the lower São Vicente Canyon. Cores NE02 and JC27-28 are located on the mouth of the Sao Vicente Canyon at the foot of the Horseshoe Fault. Core JC27-26 is located downstream of the Lagos-Portimao pathway, bounded from the Horseshoe Basin by the Horseshoe Fault; and core JC27-27 is located at the northern HAP, down the slope from the MPF block. The logs of these cores (JC27-26, JC27-27 and JC27-28) are included in Annex I.

The HAP cores, MD03 2703 and MD03 2704, are formed by a succession of 8 (T1 to T8) and 9 (T1 to T9) turbidite layers, respectively. The colour of turbidites varies from olive (5Y 4/4) to dark grey (5Y 4/1), and their thickness ranges from 4 to 140 cm (Fig. 8). The sand fraction is composed of quartz, feldspar, carbonates, micas, heavy minerals and biogenic components (50% foraminifera), which may reach 72% of the total components of this fraction. The grain-size distribution of the turbidite bases ranges from silty-clay (mean diameter of 5.8 Φ) to medium sand (mean diameter of 3.6 Φ).

In core MD03 2703, two groups of turbidites were distinguished based on their physical properties. In the upper interval (from T1 to T5), magnetic susceptibility ranges between 5 and 24 SI, density oscillates from 1.4 to 2.1 gr/cm^3. In the lower interval (T6 to T8), MS and density vary between 8 and 34 SI and 2 to 2.4 gr/cm^3, respectively. L* is characterized by a successive increase in darker colours, from 47 in T1 to 31 in T7. In core MD03 2704, there are also two groups of turbidites depending on the physical parameters. In the upper interval (from T1 to T7), magnetic susceptibility ranges between 6 and 32 SI, density oscillates from 0.8 to 2.2 gr/cm^3, and L* from 35 and 52. T4 constitutes an exception with low values of lightness (L* = 29). The lower turbidite group (T8 and T9) is characterized by MS values ranging from 8 to 50 SI, density values from 1.6 to 2.4 gr/cm^3, and the lightness reaches down to 27. In both cores, hemipelagites show average values of MS about 12 SI, increasing densities from 1.3 to 2.0 gr/cm^3 and relatively high values of L* between 45 and 55 (Fig. 8). Cores MD03 2703 and MD03 2704 also show similar trends (Fig. 8). In MD03 2703 XRF measurements performed in the turbidites show K/Ti and Ca/Ti values fluctuating between 1.3 to 2 and 10 to 35, respectively. T6 and T7 in core MD03 2703 present the highest values of K/Ti (up to 2.5) and Ca/Ti (up to 43) respectively. In core MD03 2704 turbidites show higher values of K/Ti (between 1.3 and 3.4) and Ca/Ti (between 17 and 65) with marked peaks of both ratios observed in T4, T6 and T7 (Fig. 8). In both cores, hemipelagites are characterized by detrital values ranging between 1.4 and 2.5 and calcareous values from 14 to 30.

Five Holocene turbidites (T1 to T5) and three pre-Holocene turbidites (T6 to T8) were distinguished in core MD03 2703. In the Holocene section they occurred at around 2080 – 2620 yr BP, 6340 – 6505 yr BP, 6690 – 6985 yr BP, 8185 – 8425 yr BP, and 8715 – 9015 yr BP, respectively; and during the Last Glacial-Interglacial Transition period at 12950 – 13325 yr BP, 15695 – 16090 yr BP, and 16160 – 16635 yr BP, respectively (Fig. 4c, Table 2). In core MD03 2704 the 7 uppermost turbidites (T1, T2, T3, T4, T5, T6 and T7) were deposited during the Holocene, at around 300 – 560 yr BP, 855 – 1110 yr BP, 2285 – 2415 yr BP, 6110 – 6365 yr BP, 6745 – 7020 yr BP, 7930 – 8240 yr BP and 8880 – 9090 yr BP, respectively. Turbidites T8 and T9 occurred during the Last Glacial-Interglacial

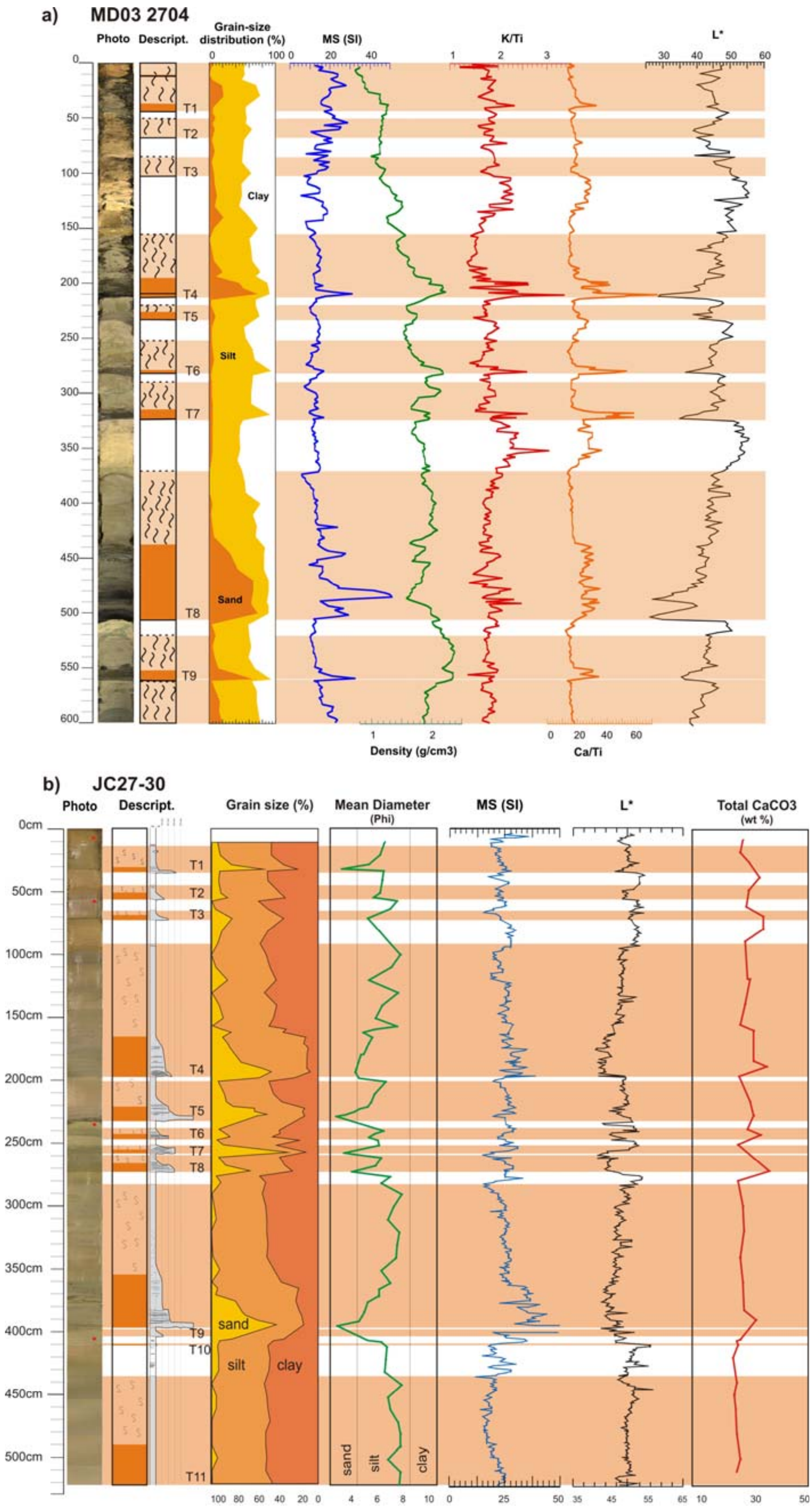

Fig. 8. *Image, lithological description, grain-size distribution, magnetic susceptibility, density and geochemical composition of the studied sections of cores MD03 2704 and JC27-30 from the Horseshoe Abyssal Plain. Turbidite numbers are depicted. See caption in Figure 5.*

Transition period at around 13430 – 13715 yr BP and 14275 – 14780 yr BP, respectively (Table 2).

Core JC27-30 with a length of 5.22 m, contains fairly regular series of 11 mud-dominated turbidites interlayered with hemipelagic intervals. Hemipelagites are composed of light grey to light brown mud layers characterized by relatively constant values of MS between 50-60 SI, and carbonate values of (24 to 34 wt%) with the exception of an hemipelagite located at 410-435 cm which shows a downward increase of total carbonate. Turbidite bases, dominated by grey sand facies and erosional bases, show planar laminations, as observed on turbidites T1, T4, T5, T7, and T9; and cross bedding structures on T4 and T7. Turbidites show a variable MS, following a downcore increasing trend of MS in each turbidite episode, from 48 to 60 S.I. Opposite trend is observed on the lightness measurements. Total calcium carbonate show variable values ranging from 22-35 wt %. In core JC27-30, the uppermost turbidites T1 to T4 were deposited during the Holocene, with ages of 1510 - 1605 yr BP for the top of T1, 1855 - 1940 yr BP for the base of T2, and 10240 - 10365 for the base of T5. Turbidites T6 to T11 occurred during the Last Glacial, as suggested by the age of 22290 - 22530 yr BP obtained at the base of T9 (Table 2).

5.5. Seine Abyssal Plain

Only one core was acquired on the SAP. Core JC27-20 was collected in the NE sub-basin of the Seine Abyssal Plain, just beyond the mouth of the Rharb Valley (Table 1). Although the whole core was 7.5 m long, we present here a section of 450 cm, containing 8 turbidites interlayered with hemipelagic intervals (Fig. 9).

Hemipelagites are composed of creamy brown to grey mud (up to 60% clay) structureless layers. They are characterized by low to medium values (between 15 and 35 SI) of magnetic susceptibility and high values of lightness (up to 60). Total Calcium carbonate content varies from 20-30% following a similar trend as the lightness. Hemipelagic intervals show abundant bioturbation with scattered foraminifera and presence of dark oxidized spots in some layers. Four hemipelagic samples were sent to NOSAMS laboratory for dating the first 4 turbidites (Table 1, Fig. 9). Once we receive the ^{14}C ages we will be able to know if these turbidites are of Holocene age and can be included in the regional correlation. Two Holocene events were distinguished in the central SAP by Davies et al. (1997).

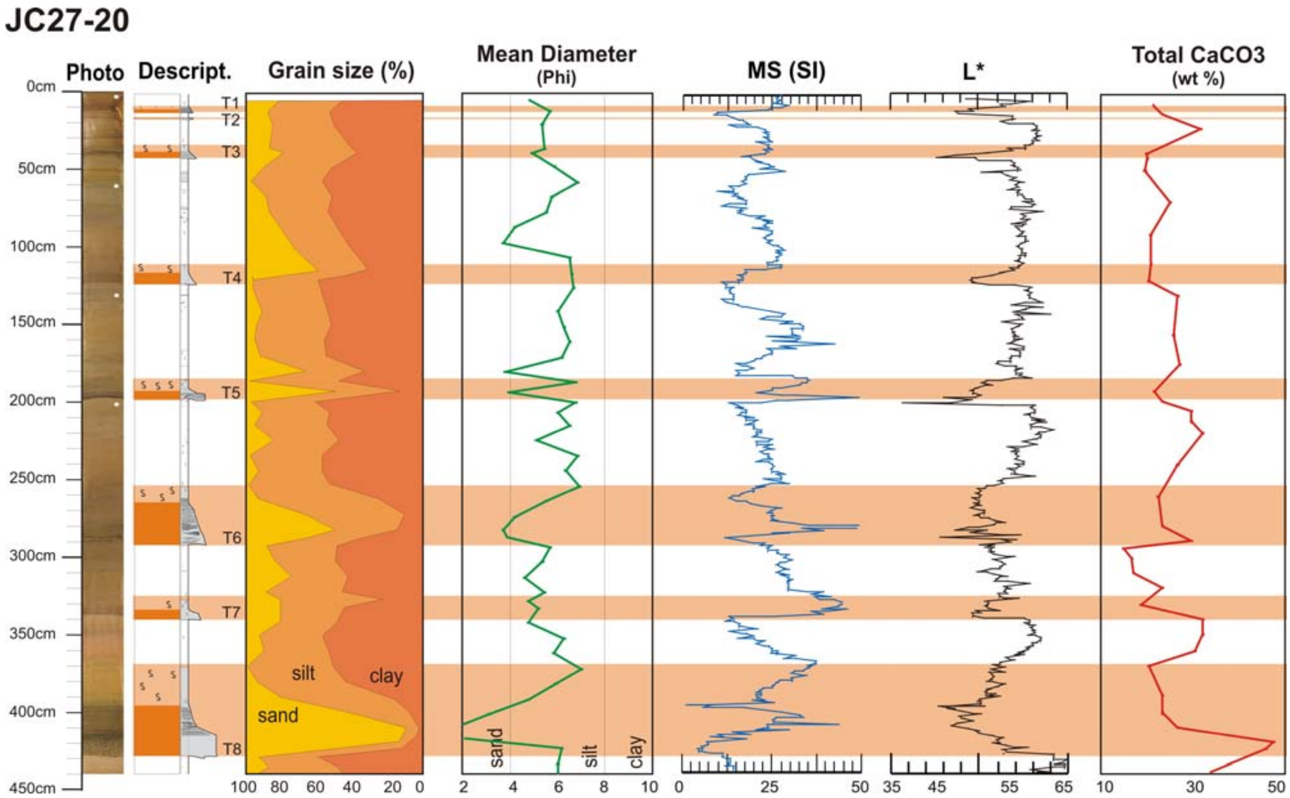

Fig. 9. *Image, lithological description, grain-size distribution, mean diameter, magnetic susceptibility, lightness and total carbonate composition of the studied sections of core JC27-20 from the Seine Abyssal Plain. Turbidite numbers are depicted. See caption in Figure 5.*

A total of 8 turbidites (T1 to T8), presumably sourced via the Rharb Valley, have been observed in the studied sections. All turbidites show sharp erosional bases and upward thinning sequences along the turbidite tails. The colour of turbidites varies from brown grey to dark grey (5Y 4/1), and their thickness ranges from few cm to 60 cm thick (Fig. 9). The grain-size distribution of the turbidite bases ranges from silty-clay (mean diameter of 5.8 Φ) to coarse sand (mean diameter of 2 Φ). Turbidite T8 is the thickest and we could differentiate the different intervals of Bouma sequence, as follows: Ta: Gray medium structureless sand, with sharp erosional base; Tb: Dark gray fine sand to medium sand planar laminations; Tc: Gray silty mud ripple cross laminations; Td: Gray to dark mud to silty mud gray planar laminations, and Te: Brown gray mud with slight bioturbation and silty spots.

In the turbidite facies, MS values ranges between 12-50 SI, with the higher values found at the turbidite bases decreasing towards the tails. Mirroring MS, lightness values are very low (35) at the dark turbidite bases showing higher values (50) towards the lighter coloured turbidite tails. Carbonate values show correspondence with lightness, suggesting that turbidite bases are rich in detrital, non-biogenic components.

6. Concluding remarks

A total of 21 sediment cores acquired in the main depositional areas (i.e. Tagus Abyssal Plain, Infante Don Henrique Basin, Horseshoe Abyssal Plain and Seine Abyssal Plain) and drainage pathways of the SW Iberian Margin provide valuable insights into the sedimentary processes of the area during the Holocene and Late Pleistocene. The abundance of turbidites intercalated between hemipelagites confirms the virew that the SW Iberian Margin is largely affected by mass transport processes.

A detailed sediment core characterization based on grain-size, physical properties and geochemical composition allows us to distinguish and characterize three main sedimentary facies: turbidites, hemipelagites and debrites. In the case of MD03 cores, an accurate chronology of turbidite deposits is based on the calibration of the ^{14}C ages from hemipelagic samples using the P_Sequence modelling approach from the computer program OxCal 4.0. This allowed us to interpolate and extrapolate the ages of the calibrated samples as far as the base or top of the neighbouring turbidite intervals, and thus provide an accurate age for each turbidite layer.

7. Acknowledgments

The work presented in this report has been carried out by Eulàlia Gràcia in collaboration with the UTM-CSIC group formed by Alexis Vizcaino, Graziella Bozzano and Zoraida Roselló. Support from Claudio Lo Iacono, Rafael Bartolomé and Susana Diez (UTM-CSIC) during WP6 activities is acknowledged. We thank David Casas (IGME, Madrid) for his help in measuring physical properties of cores SW-2004 and NE-2007 using the MSCL GEOTEK of the ICM-CSIC (Barcelona). Preparation of the samples and picking of foraminifera species for dating has been carried out by Alessandra Asioli (CNR-Padova). Angel Rodés and Raimon Pallàs (UB, Barcelona) helped on the chronological model for cores MD03. We thank Nevio Zitellini and Gabriella Carrara (CNR-ISMAR, Bologna) for their collaboration in collecting the SWIM-2004 (SW) and NEAREST-2007 (NE) sediment cores presented here. We also thank Russell Wynn and Douglas Masson (NOCS, United Kingdom) for its invitation to collaborate in planning, acquiring and working on the sediment cores from the Gulf of Cadiz collected during the JC27 cruise. We wish to thank the captain, crew, scientific and technical staff on board the RV Marion Dufresne (France), RV Urania (Italy) and RV James Cook (UK).

8. References

Adams, J., 1990. Paleoseismicity of the Cascadia subduction zone: Evidence from turbidites off the Oregon-Washington margin. Tectonics 9, 569-583.

Argus, D.F., Gordon, R.G., DeMets, C., Stein, S., 1989. Closure of the Africa-Eurasia-North America plate motion circuit and tectonics of the Gloria Fault. Journal of Geophysical Research 94, 5585-5602.

Baptista, M.A., Heitor, S., Miranda, J.M., Miranda, P., Mendes Victor, L., 1998. The 1755 Lisbon Tsunami; Evaluation of the tsunami parameters. Journal of Geodynamics 25 (2), 143-157.

Bronk Ramsey, C., 2008. Deposition models for chronological records. Quaternary Science Reviews 27, 42–60.

Buforn, E., Sanz de Galdeano, C., Udías A., 1995. Seismotectonics of the Ibero-Maghrebian region. Tectonophysics 248, 247-261.

Buforn, E., Bezzeghoud, M., Udías, A., Pro, C., 2004. Seismic sources on the Iberia-African Plate boundary and their Tectonic Implications. Pure and Applied Geophysics 161, 623-646.

Davies, T.L., B. Van Niel, B., Kidd, R.B., Weaver, P.P.E., 1997. High-resolution stratigraphy and turbidite processes in the Seine Abyssal Plain, northwest Africa. Geo-Marine Letters 17, 147-153.

Fukao, Y., 1973. Thrust faulting at a lithospheric plate boundary: The Portugal earthquake of 1969. Earth and Planetary Science Letters 18, 205-216.

Garcia-Orellana, J., Gràcia, E., Vizcaino, A., Masqué, P., Olid, C., Martínez-Ruiz, F., Piñero, E., Sanchez-Cabeza, J.A., Dañobeitia, J.J., 2006. Identifying instrumental and historical earthquake records in the SW Iberian Margin using 210Pb turbidite chronology. Geophysical Research Letters 33, L24601.

Goldfinger, C., Nelson, C.H., Johnson, J.E., Shipboard Scientific Party, 2003. Holocene earthquake records from the Cascadia subduction zone and northern San Andreas Fault based on precise dating of offshore turbidites. Annual Reviews of Earth and Planetary Science 31, 555-577.

Goldfinger, C., Morey, A.E., Nelson, C.H., Gutiérrez-Pastor, J., Johnson, J.E., Karabanov, E., Chaytor, J., Eriksson, A., 2007. Rupture lengths and temporal history of significant earthquakes on the offshore and north coast segments of the Northern San Andreas Fault based on turbidite stratigraphy. Earth and Planetary Science Letters 254 (1-2), 9-27.

Gràcia, E., Dañobeitia, J.J., Vergés, J., PARSIFAL Team 2003a. Mapping active faults offshore Portugal (36ºN-38ºN): Implications for seismic hazard assessment along the southwest Iberian margin. Geology 31(1), 83-86.

Gràcia, E., Dañobeitia, J.J., Vergés, J., Bartolomé, R., Córdoba, D., 2003b. Crustal architecture and tectonic evolution of the Gulf of Cadiz (SW Iberian Margin) at the convergence of the Eurasian and African Plates. Tectonics 22(4), 1033-1058.

Gràcia, E., Pallàs, R., Soto, J.I., Comas, M., Moreno, X., Masana, E., Santanach, P., Diez, S., García, M., Dañobeitia, J.J., 2006. Active faulting offshore SE Spain (Alboran Sea): Implications for earthquake hazard assessment in the Southern Iberian Margin. Earth and Planetary Science Letters 241 (3-4), 734-749.

Grimison, N.L., Chen, W.P., 1986. The Azores-Gibraltar Plate Boundary: Focal Mechanisms, Depths of Earthquakes and their Tectonic Implications. Journal of Geophysical Research 91 (B2), 2029-2047.

Gutiérrez-Pastor, J., Nelson, C.H., Goldfinger, C., Johnson, J.E., Escutia, C., Eriksson, A., Morey, A.E., and the Shipboard Scientific Party, 2009. Earthquake control of Holocene turbidite frequency confirmed by hemipelagic sedimentation chronology on the Cascadia and Northern California active tectonic continental margins. In: Kneller, B., McCaffrey, W., Martinsen, O.J. (Eds.), External Controls on Deepwater Depositional Systems. SEPM Special Publication, v. 92. Society for Sedimentary Geology, Tulsa, OK, ISBN 978-1-56576-136-0, p. 179–197.

Hayward, N., Watts, A.B., Westbrook, G.K., Collier, J., 1999. A seismic reflection and GLORIA study of compressional deformation in the Gorringe Bank, eastern North Atlantic. Geophysical Journal International 138, 831-850.

Lebreiro, S.M., McCave, I.N., Weaver, P.P.E., 1997. Late quaternary turbidite emplacement on the Horseshoe Abyssal Plain (Iberian Margin). Journal of Sedimentary Research 67 (5), 856-870.

Martínez Solares, J.M., López Arroyo, A., 2004. The Great historical 1755 earthquake: Effects and damage in Spain. Journal of Seismology 8, 275-294.

Masana, E., Martínez-Díaz, J.J., Hernández-Enrile, J.L., Santanach. P., 2004. The Alhama de Murcia fault (SE Spain), a seismogenic fault in a diffuse plate boundary: Seismotectonic implications for the Ibero–Magrebian region. Journal of Geophysical Research 109, 1–17.

McClusky, S., Reilinger, R., Mahmoud, S., Ben Sari, D., Tealeb, A., 2003. GPS constraints on Africa (Nubia) and Arabia plate motions. Geophysical Journal International 155 (1), 126–138.

Monge Soares, A.M., Alveirinho Dias, J.M., 2006. Coastal upwelling and radiocarbon-Evidences for temporal fluctuations in ocean reservoir effect off Portugal during the Holocene. Radiocarbon 48 (1), 45-60.

Nelson, C.H., Goldfinger, C., Vallier, T.L., McGann, M.L., Kashgarian, M., 1996. North to south variation in Cascadia Margin turbidite event history: implications for paleoseismicity. Geological Society of America, Abstracts with programs 28 (5), 95.

Peláez, J.A., López Casado, C., 2002. Seismic hazard estimate at the Iberian Peninsula. Pure and Applied Geophysics. 159, 2699–2713.

Reimer, PJ; Baillie, MGL; Bard, E; Bayliss, A; Beck, JW; Blackwell, PG; Bronk Ramsey, C; Buck, CE; Burr, GS; Edwards, RL; Friedrich, M; Grootes, PM; Guilderson, TP; Hajdas, I; Heaton, TJ; Hogg, AG; Hughen, KA; Kaiser, KF; Kromer, B; McCormac, FG; Manning, SW; Reimer, RW; Richards, DA; Southon, JR; Talamo, S; Turney, CSM; van der Plicht, J; Weyhenmeyer, CE, 2009. IntCal09 and Marine09 Radiocarbon Age Calibration Curves, 0–50,000 Years cal BP. Radiocarbon 51, 1111-1150

Rosas, F.M., Duarte, J.C., Terrinha, P., Valadares, V., Matias, L., 2009. Morphotectonic characterization of major bathymetric lineaments in Gulf of Cadiz (Africa-Iberia plate boundary): Insights from analogue modelling experiments. Marine Geology, 261 (1-4), 33-47.

Sartori, R., Torelli, L., Zitellini, N., Peis, D., Lodolo, E., 1994. Eastern segment of the Azores-Gibraltar line (central-eastern Atlantic): An oceanic plate boundary with diffuse compressional deformation. Geology 22, 555-558.

Skinner, L.C., and McCave, I.N. 2003. Analysis and modelling of gravity- and piston coring based on soil mechanics. Marine Geology 199 (1-2), 181-204.

Stich, D., Mancilla, F., Morales, J., 2005a. Crust-mantle coupling in the Gulf of Cadiz (SW Iberia). Geophysical Research Letters 32, L13306.

Stich, D., Batlló, J., Macià, R., Teves-Costa, Paula., Morales, J., 2005b. Moment Tensor inversion with single-component historical seismograms: 1909 Benavente (Portugal) and Lambesc (France) earthquakes. Geophysical Journal International 162, 850-858.

Stich, D., Mancilla, F. de L., Pondrelli, S., Morales, J., 2007. Source analysis of the February 12th 2007, Mw 6.0 Horseshoe earthquake: Implications for the 1755 Lisbon earthquake. Geophysical Research Letters 34, L12308.

Terrinha, P., Pinheiro, L.M., Henriet, J.P., Matias, L., Ivanov, M.K., Monteiro, J.H., Akhmetzhanov, A., Volkonskaya, A., Cunha, T., Shaskin, P., Rovere, M., 2003. Tsunamigenic-seismogenic structures, neotectonics, sedimentary processes and slope instability on the southwest Portuguese Margin. Marine Geolology 195(1-4), 55-73.

Terrinha, P., Matias, L., Vicente, J., Duarte, J., Luís, J., Pinheiro, L., Lourenço, N., Diez, S., Rosas, F., Magalhães, V., Valadares, V., Zitellini, N., Roque, C., Mendes Víctor, L., MATESPRO Team, 2009. Morphotectonics and strain partitioning at the Iberia–Africa plate boundary from multibeam and seismic reflection data. Marine Geology, 267, 156-174.

Thomson, J., Weaver, P.P.E., 1994. An AMS radiocarbon method to determine the emplacement time of recent deep-sea turbidites. Sedimentary Geology 89, 1-7.

Udías, A., López Arroyo, A., Mezcua, J., 1976. Seismotectonics of the Azores-Alboran Region. Tectonophysics 31, 259-289.

Vizcaino, A., Gràcia, E., Pallàs, R., Garcia-Orellana, J., Escutia, C., Casas, D., Willmott, V., Diez, S., Asioli, A., Dañobeitia, J.J., 2006. Sedimentology, physical properties and ages of mass-transport deposits associated to the Marquês de Pombal Fault, Southwest Portuguese Margin. Norwegian Journal of Geology 86, 177-186.

Zitellini, N., Mendes, L., Córdoba, D., Dañobeitia, J.J., Nicolich, R., Pellis, G., Ribeiro, A., Sartori, R., Torelli L., BIGSETS Team, 2001. Source of the 1755 Lisbon Earthquake and Tsunami Investigated. EOS. Transactions of AGU 82(26), 285-291.

Zitellini, N., Rovere, M., Terrinha, P., Chierici, F., Matias, L., BIGSETS Team, 2004. Neogene through Quaternary tectonic reactivation of SW Iberian Passive Margin. Pure and Applied Geophysics 161, 565-587.

Zitellini, N., Gràcia, E., Matias, L., Terrinha, P., Abreu, M.A., DeAlteriis, G., Henriet, J.P., Dañobeitia, J.J., Masson, D.G., Mulder, T., Ramella, R., Somoza, L., Diez, S., 2009. The Quest for the Africa-Eurasia plate boundary west of the Strait of Gibraltar. Earth and Planetary Science Letters 280, 13–50.

ANNEX I:

Image, lithological description, grain-size distribution, mean diameter, standard deviation, magnetic susceptibility, lightness and total calcium carbonate of cores JC27-22, JC27-23, JC27-25, JC27-26, JC27-27, JC27-28, JC27-31, JC27-32, JC27-33, JC27-34.

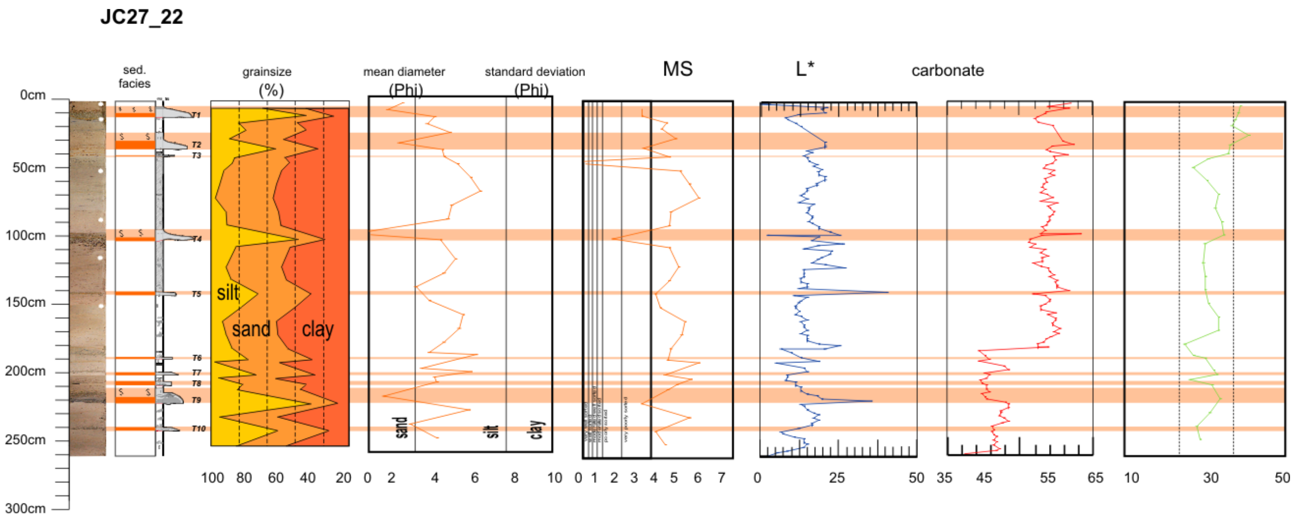

JC27_23

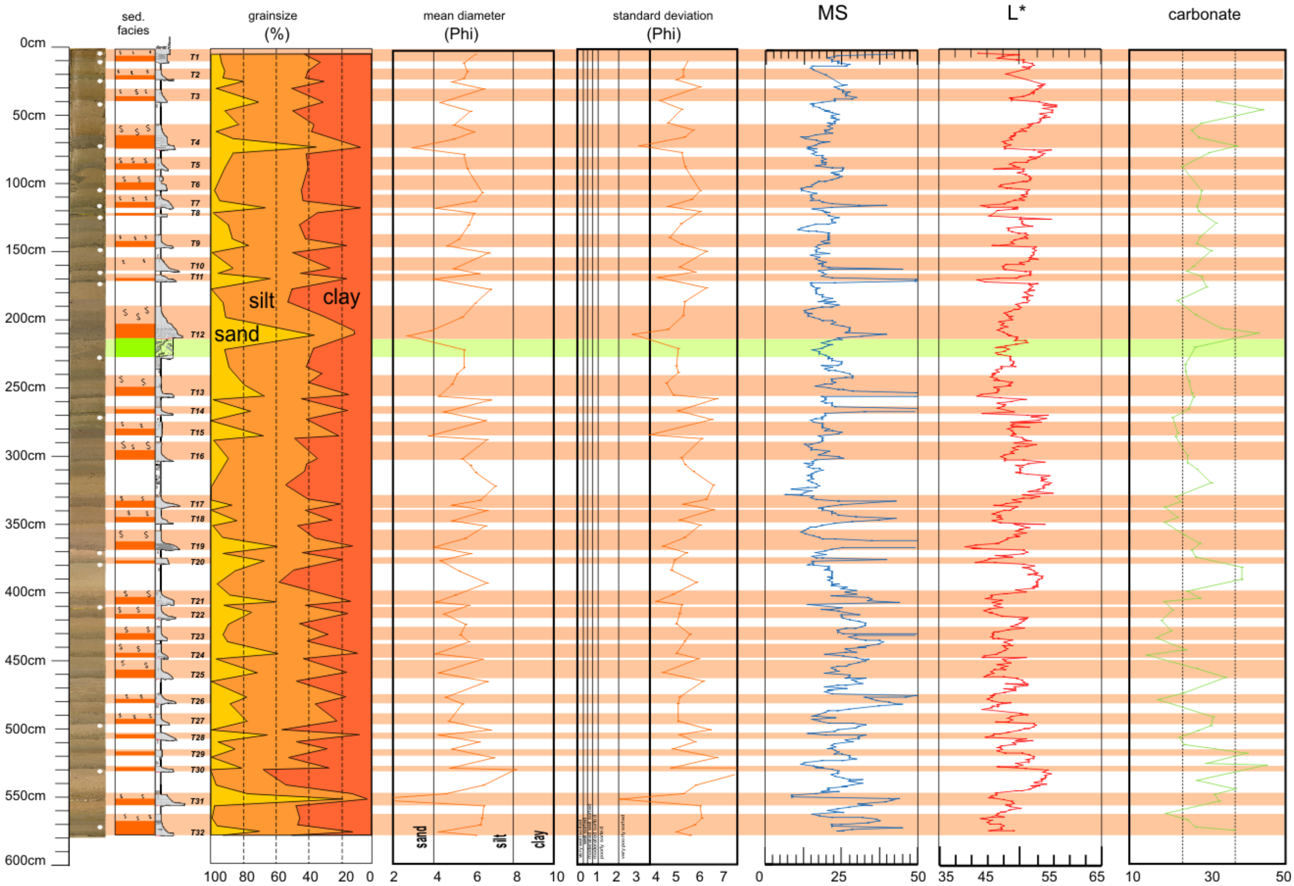
sed. facies
grainsize
(%)
mean diameter
(Phi)
standard deviation
(Phi)
MS
L*
carbonate
0cm
50cm
100cm
150cm
200cm
250cm
300cm
350cm
400cm
450cm
500cm
550cm
600cm
sand
silt
clay
T1
T2
T3
T4
T5
T6
T7
T8
T9
T10
T11
T12
T13
T14
T15
T16
T17
T18
T19
T20
T21
T22
T23
T24
T25
T26
T27
T28
T29
T30
T31
T32
100 80 60 40 20 0
2 4 6 8 10
0 1 2 3 4 5 6 7
0 25 50
35 45 55 65
10 30 50

JC27_25#3

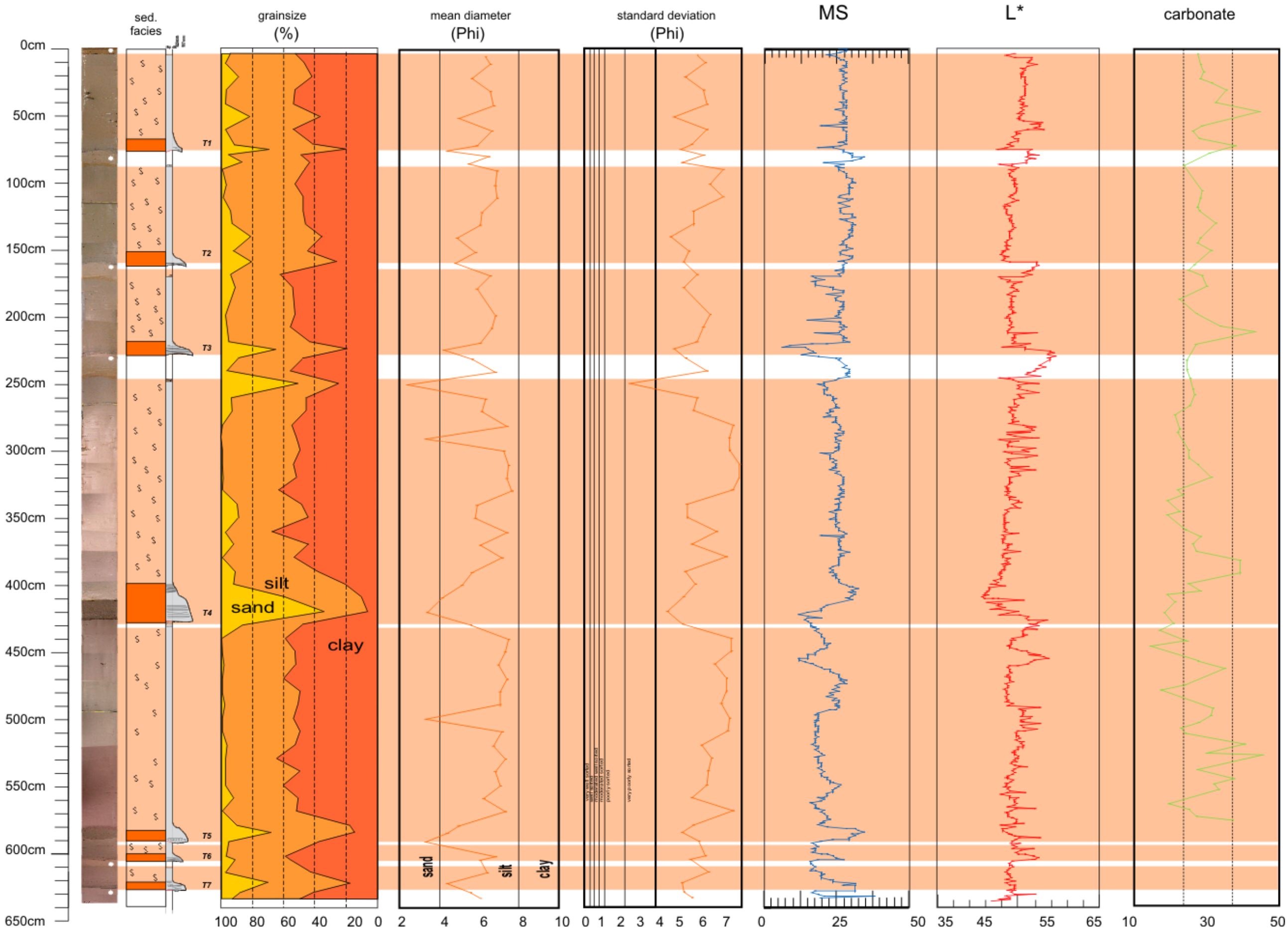

sed. facies
grainsize (%)
mean diameter (Phi)
standard deviation (Phi)
MS
L*
carbonate
0cm
50cm
100cm
150cm
200cm
250cm
300cm
350cm
400cm
450cm
500cm
550cm
600cm
650cm
T1
T2
T3
T4
T5
T6
T7
silt
sand
clay
100 80 60 40 20 0
2 4 6 8 10
sand
silt
clay
0 1 2 3 4 5 6 7
0 25 50
35 45 55 65
10 30 50

JC27_26

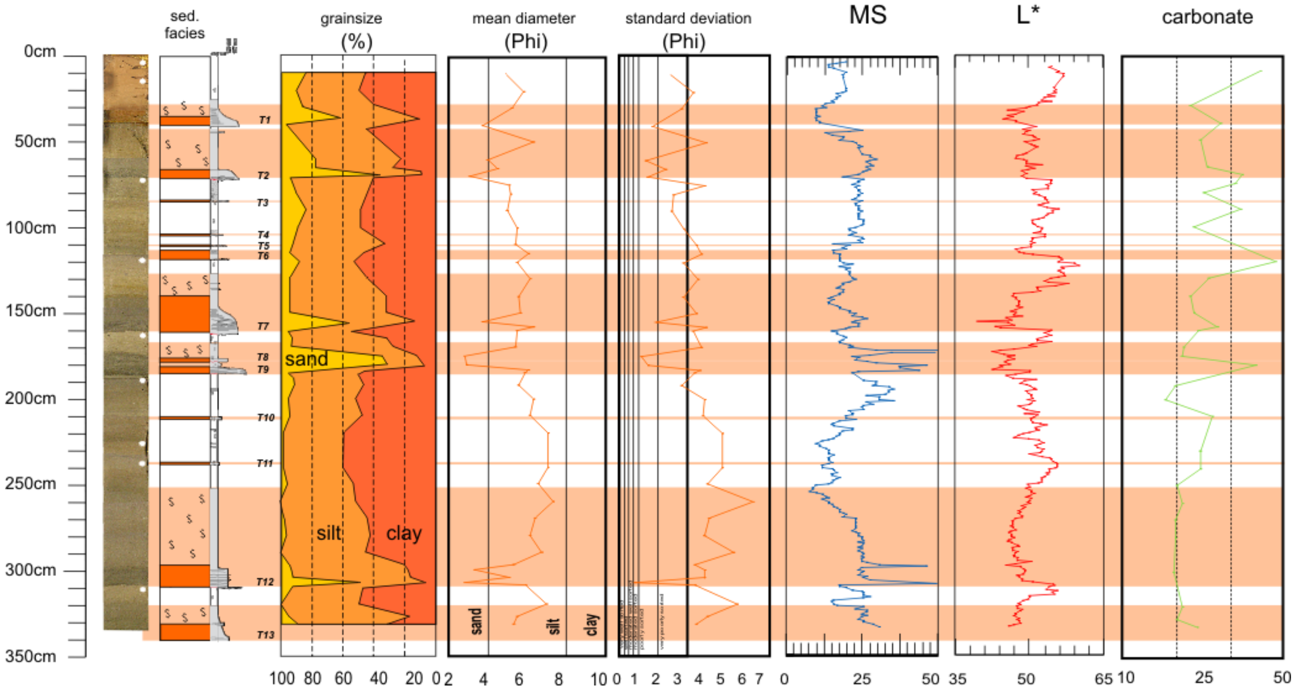

sed. facies
grainsize (%)
mean diameter (Phi)
standard deviation (Phi)
MS
L*
carbonate
0cm
50cm
100cm
150cm
200cm
250cm
300cm
350cm
T1
T2
T3
T4
T5
T6
T7
T8
T9
T10
T11
T12
T13
sand
silt
clay
100 80 60 40 20 0
2 4 6 8 10
0 1 2 3 4 5 6 7
0 25 50
35 50 65
10 25 50

JC27_27

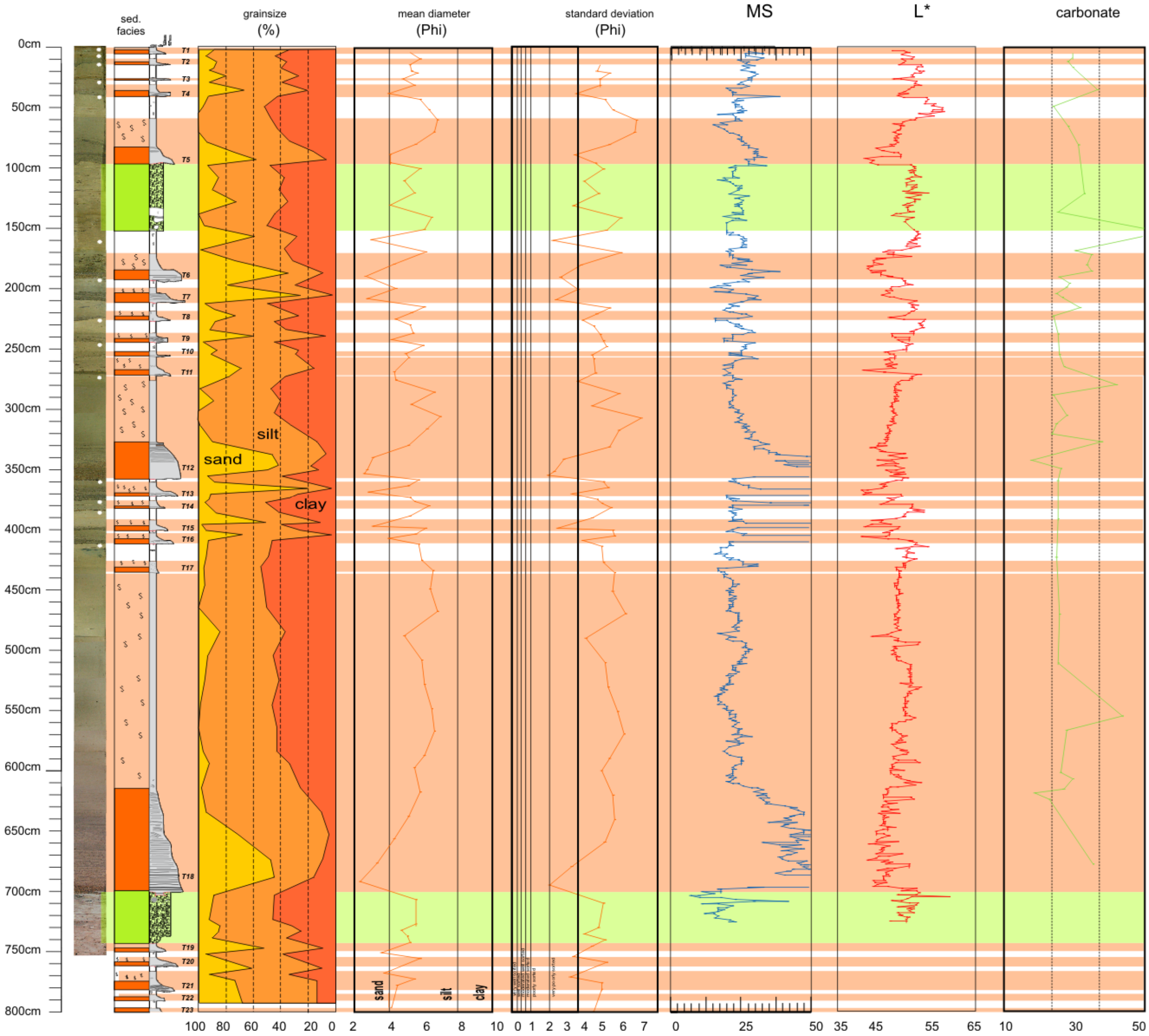

sed. facies
grainsize (%)
mean diameter (Phi)
standard deviation (Phi)
MS
L*
carbonate
0cm
50cm
100cm
150cm
200cm
250cm
300cm
350cm
400cm
450cm
500cm
550cm
600cm
650cm
700cm
750cm
800cm
sand
silt
clay
T1
T2
T3
T4
T5
T6
T7
T8
T9
T10
T11
T12
T13
T14
T15
T16
T17
T18
T19
T20
T21
T22
T23
100 80 60 40 20 0
2 4 6 8 10
0 1 2 3 4 5 6 7
0 25 50
35 45 55 65
10 30 50

JC27_28

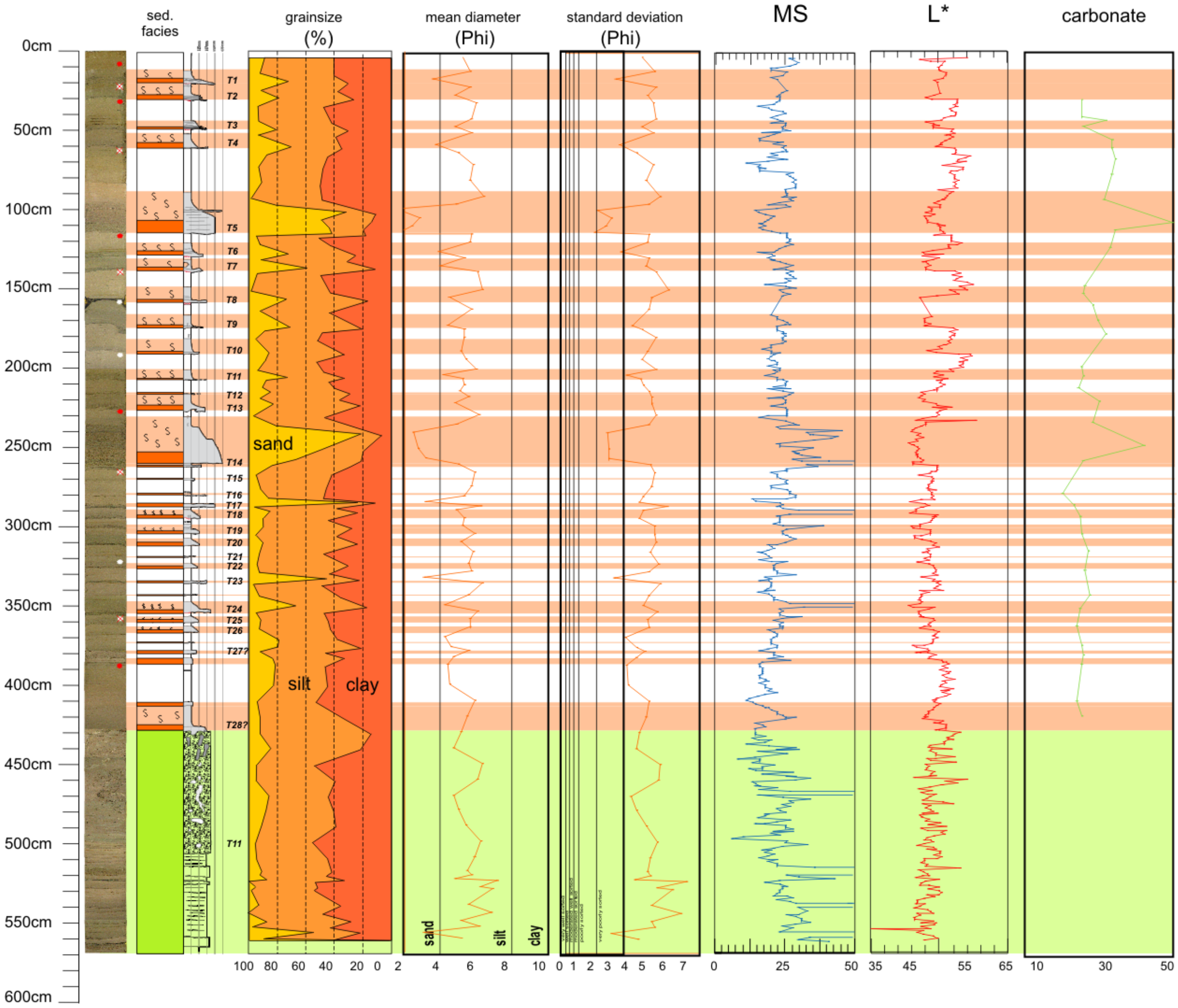
sed. facies
grainsize (%)
mean diameter (Phi)
standard deviation (Phi)
MS
L*
carbonate
0cm
50cm
100cm
150cm
200cm
250cm
300cm
350cm
400cm
450cm
500cm
550cm
600cm
T1
T2
T3
T4
T5
T6
T7
T8
T9
T10
T11
T12
T13
T14
T15
T16
T17
T18
T19
T20
T21
T22
T23
T24
T25
T26
T27?
T28?
T11
sand
silt
clay
100 80 60 40 20 0
2 4 6 8 10
0 1 2 3 4 5 6 7
0 25 50
35 45 55 65
10 30 50

JC27_31

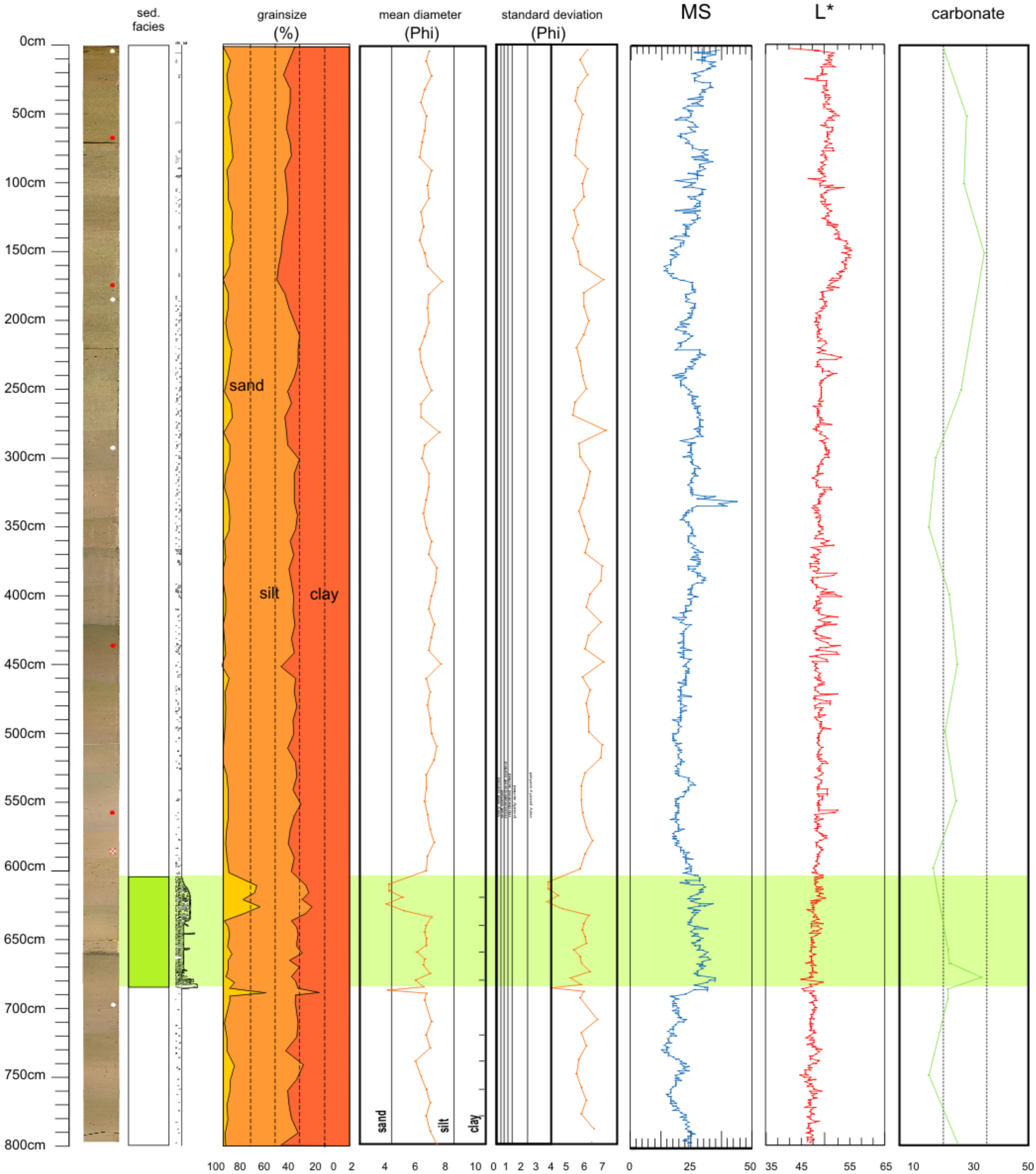

sed. facies
grainsize (%)
mean diameter (Phi)
standard deviation (Phi)
MS
L*
carbonate
0cm
50cm
100cm
150cm
200cm
250cm
300cm
350cm
400cm
450cm
500cm
550cm
600cm
650cm
700cm
750cm
800cm
sand
silt
clay
100 80 60 40 20 0
2 4 6 8 10
0 1 2 3 4 5 6 7
0 25 50
35 45 55 65
10 30 50

JC27_32

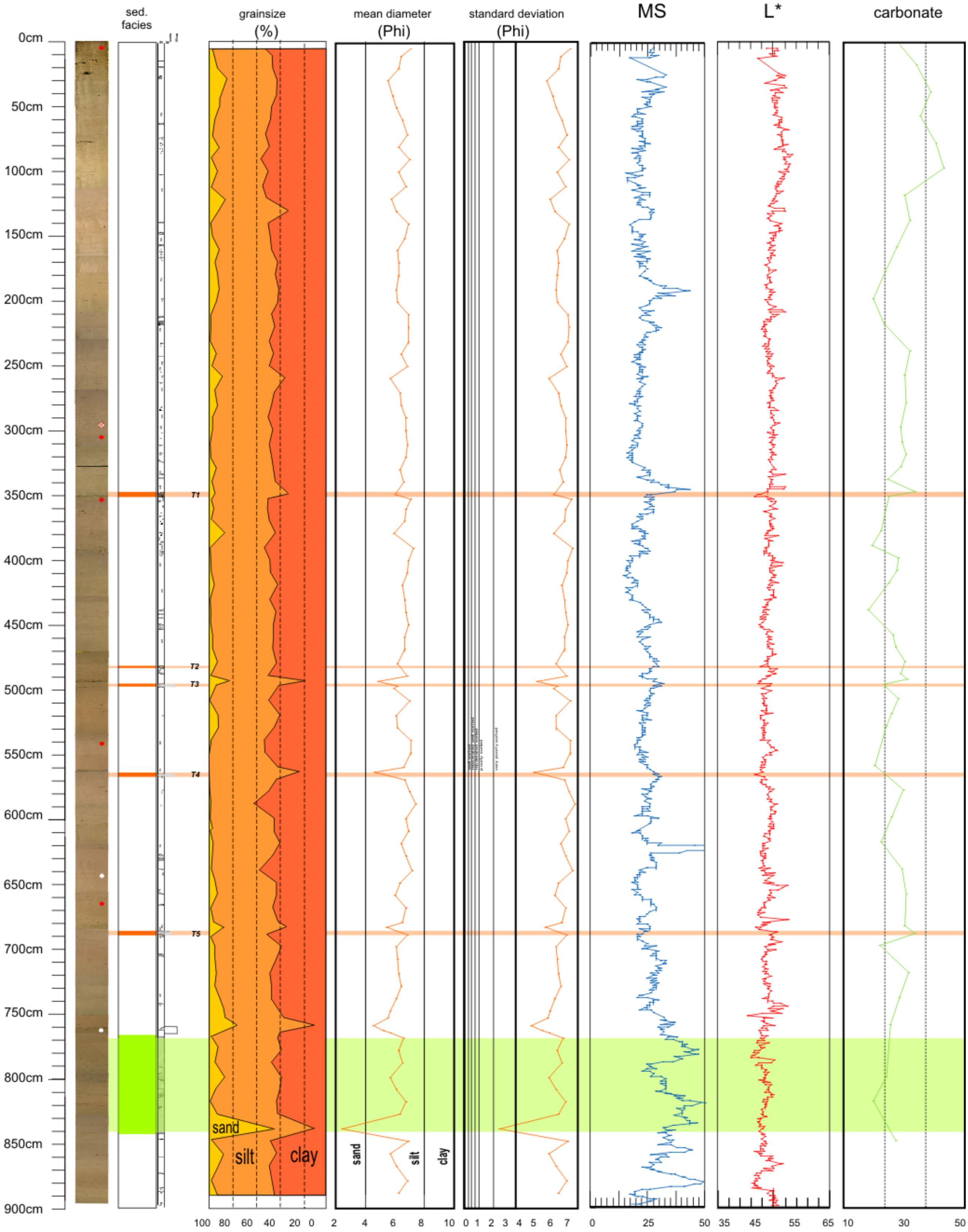
sed. facies
grainsize (%)
mean diameter (Phi)
standard deviation (Phi)
MS
L*
carbonate
0cm
50cm
100cm
150cm
200cm
250cm
300cm
350cm
400cm
450cm
500cm
550cm
600cm
650cm
700cm
750cm
800cm
850cm
900cm
T1
T2
T3
T4
T5
sand
silt
clay
100 80 60 40 20 0
2 4 6 8 10
0 1 2 3 4 5 6 7
0 25 50
35 45 55 65
10 30 50

JC27_33

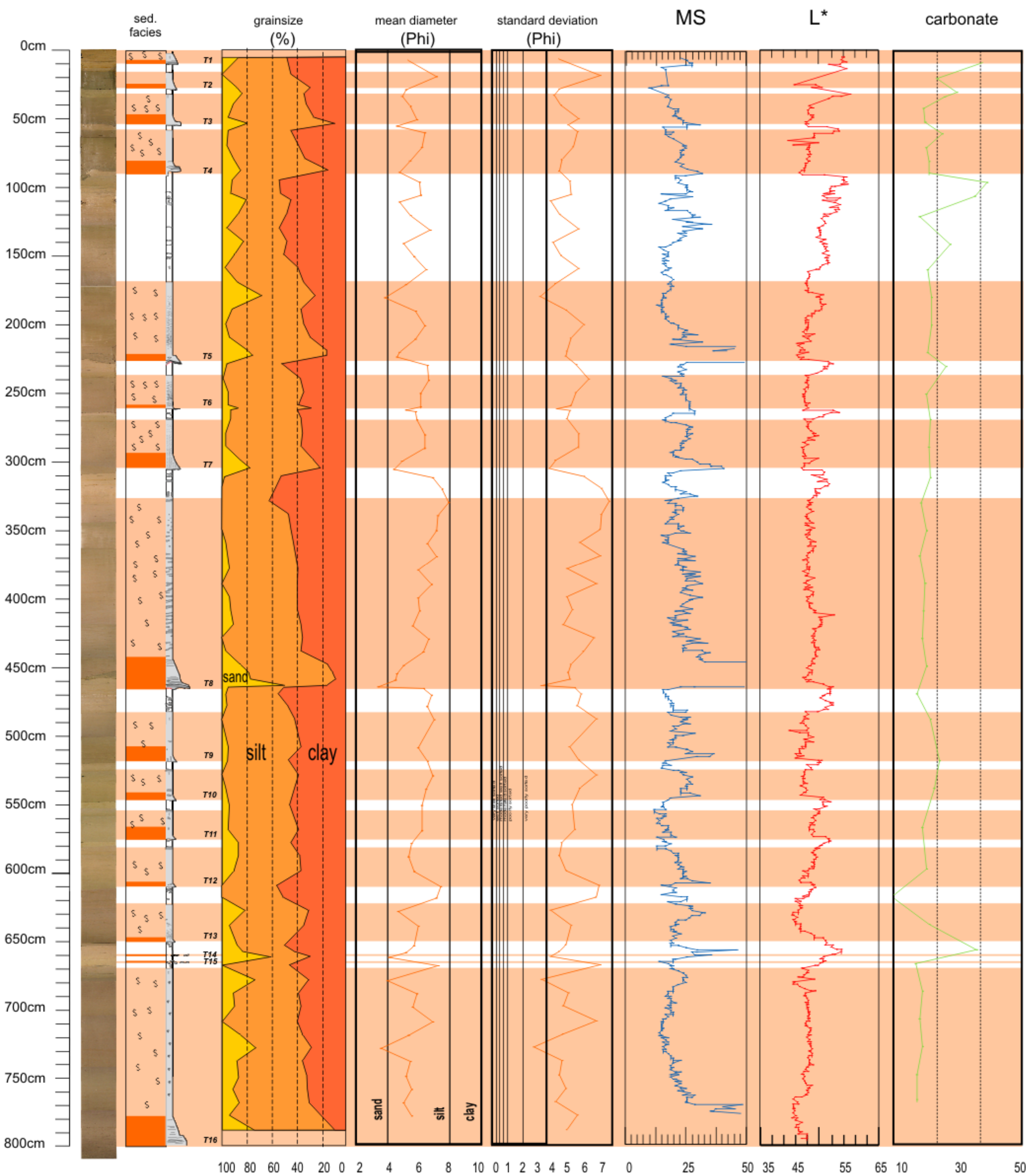

sed. facies
grainsize (%)
mean diameter (Phi)
standard deviation (Phi)
MS
L*
carbonate
0cm
50cm
100cm
150cm
200cm
250cm
300cm
350cm
400cm
450cm
500cm
550cm
600cm
650cm
700cm
750cm
800cm
T1
T2
T3
T4
T5
T6
T7
T8
T9
T10
T11
T12
T13
T14
T15
T16
sand
silt
clay
100 80 60 40 20 0
2 4 6 8 10
0 1 2 3 4 5 6 7
0 25 50
35 45 55 65
10 30 50

JC27_34

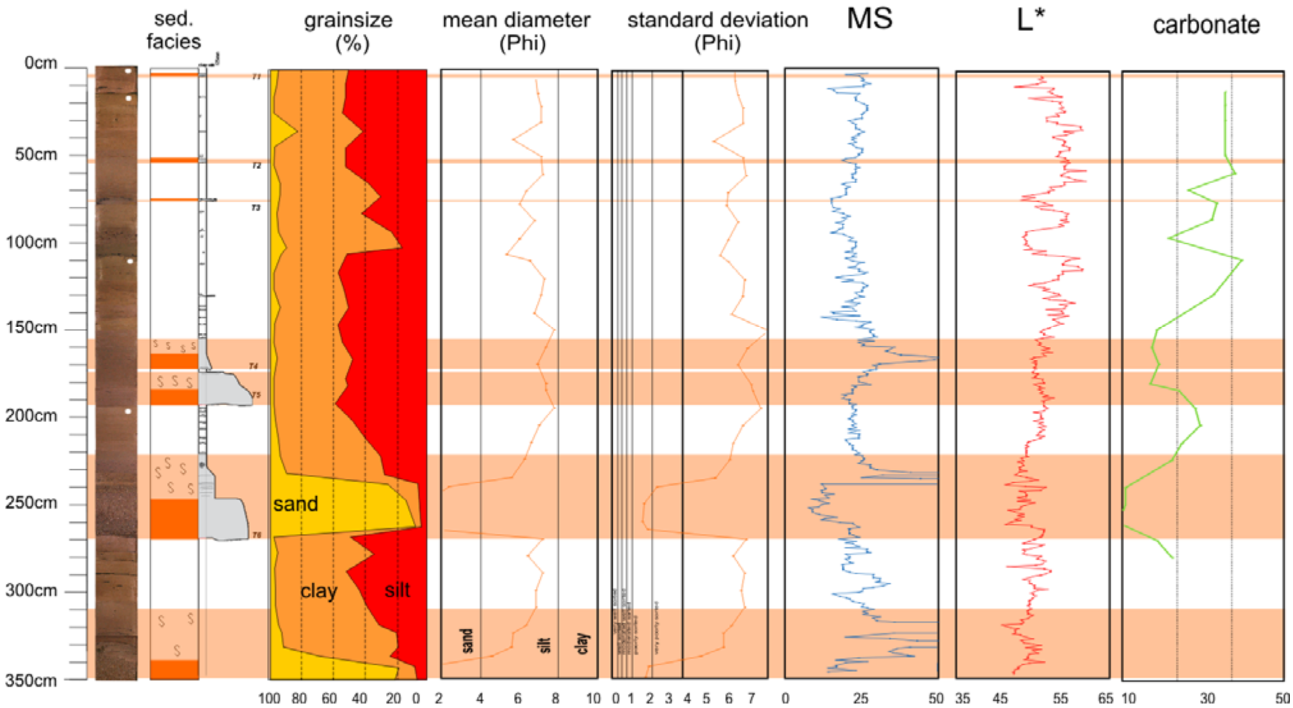
sed. facies
grainsize (%)
mean diameter (Phi)
standard deviation (Phi)
MS
L*
carbonate
0cm
50cm
100cm
150cm
200cm
250cm
300cm
350cm
sand
clay
silt
sand
silt
clay
100 80 60 40 20 0
2 4 6 8 10
0 1 2 3 4 5 6 7
0 25 50
35 45 55 65
10 30 50